

Algorithms for controlling and tracking UAVs in indoor scenarios



Andrea Nisticò

Supervised by: Marco Baglietto, Fulvio Mastrogiovanni

DIBRIS - Department of Informatics, Bioengineering, Robotics,
and Systems Engineering

University of Genova

In partial fulfillment of the requirements for the degree of

Robotics Engineering

September 18, 2015

Acknowledgements

Don't forget to acknowledge your supervisor!

To all the Master and PhD students of Robotics Engineering at the
University of Genova.

Abstract

Quadcopter, also known as quadrotor, is a helicopter with four rotors. The rotors are directed upwards and they are placed in a square formation with equal distance from the center of mass of the quadcopter. The quadcopter is controlled by adjusting the angular velocities of the rotors which are driven by electric motors. An on board autopilot, namely PiXHawk with PX4 software, pack all the interfaces for sensors, motor controllers and radio antennas. It also manages the control, state estimation and signals processing. The goal of this master thesis is to develop algorithms for UAV trajectory planning and execution (as well as the related SW components), using the motion capture system as the source of the UAV position feedback. An IRIS quadrotor is used from 3d Robotics. After an introduction to the components, the integration between them both hardware and software is presented. The model of the IRIS is briefly derived and explained as well as the control techniques involved in the open source autopilot. Moreover a software architecture is presented where a task based program is able to read a set of tasks from a list and let the robot execute them sending position set point through radio link. At the end an algorithm for tracking and landing on a mobile platform is explained and the overall results are presented.

Contents

1	Introduction	1
1.1	Overview	1
1.1.1	Hosting laboratories	2
1.2	Problem statement	3
1.2.1	Work plan	3
2	Related work	4
2.1	Quadrotor platform	4
2.2	Motion capture systems	7
2.3	Current autopilots	8
2.4	Modeling and control	9
2.5	Software architectures and control stations	12
2.6	Landing on a moving platform	13
3	System description	16
3.1	The setup	16
3.1.1	IRIS Quadcopter	17
3.1.1.1	PixHawk board	18
3.1.1.2	PX4 Autopilot	19
3.1.1.3	MAVLink Protocol	20
3.1.2	Motion capture system	22
3.1.2.1	Image sensor specifications and performances . .	22
3.1.2.2	Software, cameras layout and requirements . . .	23
3.1.3	Flight Arena	25
3.2	Overall Integration	26
3.2.1	Hardware interfaces	26
3.2.2	Software interfaces	29
3.2.2.1	Adapting reference frames	29

CONTENTS

4 Modeling IRIS	33
4.1 Generalities	33
4.1.1 Reference frames	33
4.1.2 General assumptions	34
4.2 Transformation matrices	35
4.3 Propulsion and controls	37
4.4 Complete model	40
4.4.1 Rigid body equations	40
5 Control and state estimation	45
5.1 Introduction to the PX4 Flight Stack	45
5.1.1 Message pass-through	45
5.1.2 Onboard nodes	46
5.1.3 State machine overview	48
5.2 Estimation modules	49
5.2.1 Position estimator	49
5.2.2 Attitude estimator	50
5.3 Controller architecture	52
5.3.1 Position controller	53
5.3.2 Velocity controller	54
5.3.3 Attitude controller	55
5.4 Results and validation	56
5.4.1 Estimator validation	56
5.4.2 Controller results	58
6 Software architecture	63
6.1 Introduction to the proposed architecture	63
6.2 Design patterns	63
6.3 Software description	63
6.4 Experiments and results	63
7 Landing on a mobile platform	64
8 Results	65
9 Conclusions	66
A Extra	67
References	72

List of Figures

1.1	Different applications of multirotors	2
2.1	Predator UAV	5
2.2	Motion capture stage	8
3.1	The IRIS quad copter	17
3.2	IRIS and control devices	18
3.3	Pixhawk board	19
3.4	Ground Control Station	20
3.5	MAVLink package anatomy	22
3.6	Flex 13 Cameras	23
3.7	Passive IR marker	24
3.8	Single hub connection	24
3.9	IRIS Rigid body	25
3.10	Marker placement on IRIS	26
3.11	Flight arena	27
3.12	Flight arena panoramic	28
3.13	Flight arena from motive	29
3.14	Telemetry module	30
3.15	Setup scheme	31
3.16	NED and Mocap frames	32
4.1	Reference frames for modeling	34
4.2	Blade flapping	35
4.3	Motor rotations	38
4.4	Quad dynamics	39
5.1	Publish/Subscribe design pattern.	46
5.2	IRIS state machine	48
5.3	Controller overall structure.	53
5.4	Roll estimation	56
5.5	Pitch estimation	57

LIST OF FIGURES

5.6	Yaw estimation	58
5.7	Convergence on x	59
5.8	Convergence on y	59
5.9	Convergence on z	60
5.10	Yaw tracking	61
5.11	Static hover with external perturbations	62

Chapter 1

Introduction

Summary

This chapter will introduce the reader to the topic of this master thesis. It will present the work plan and at the end a technical description of the equipment used, the specifications of each component and how it is interfaced with the overall setup.

1.1 Overview

In the latest years, aerial robotics has grown so fast both in technology and popularity among the public and multirotor aircrafts such as quadcopters are one of the most promising fields. In fact those type of vehicles have become a standard platform for research in many laboratories , driven by totally different customer needs the research improved substantially. They have sufficient payload and flight endurance to support a number of indoor and outdoor applications, and the improvements of battery and other technology is rapidly increasing the scope for commercial opportunities. They are highly maneuverable and enable safe and low-cost experimentation in mapping, navigation, and control strategies for robots that move in three-dimensional space. Small quadrotors have been demonstrated for exploring and mapping 3-D environments; transporting, manipulating, and assembling objects; and acrobatic tricks such as juggling, balancing, and flips.

As stated before, the uses of this platform are many and limited only by the imagination of the designers. Figure 1.1 illustrates various application going from search and rescue to public defense, most of them in outdoor scenarios. Very interesting is to investigate the possible use of this technology in an indoor scene where the comforting signal of the GPS is not present and analyze every aspect

1.1 Overview



Figure 1.1: Different applications of multirotors

of flight going from state estimation, control and stability to autonomy, path planning and high level automation.

This work investigates the integration between different heterogeneous entities as well as the possibility to design a safe, reliable and flexible architecture capable of letting the robot navigate safely in a closed environment. At the end a simple algorithm for landing on a mobile platform is presented with very interesting results demonstrating the potential of this setup.

1.1.1 Hosting laboratories

This thesis is carried out as a cooperation between the Laboratorium Lab (focus: autonomous robotics and ambient intelligence), the NOCC Lab (focus: control, identification and estimation) and the upcoming joint EMARO@DIBRIS Lab.

1.2 Problem statement

The goal of this master thesis is to develop algorithms for UAV trajectory planning and execution (as well as the related SW components), using the motion capture system as the source of the UAV position feedback. Once achieved stability more complex aspect are investigated, a task based software architecture is presented and a simple technique for landing on a mobile platform is proposed.

The above stated, is formulated in to the following problem statement for the project:

It is possible, through position feedback given from a motion capture system, to design a set of algorithms and SW components enabling the IRIS to achieve stability and perform different tasks in an indoor scenario?

1.2.1 Work plan

The work got through several tasks covering all aspects, they can be distinctly divided in main blocks hence defining the work plan.

1. Analysis of state of the art approaches to UAV control, modeling, trajectory planning and execution
2. Technical analysis and documentation on the given tools (Autopilot, Motion Capture, IRIS Quadcopter)
3. Integration between mocap and IRIS
 - Integration and testing between mocap and onboard estimation modules
 - Integration and testing of onboard controller through set point control
4. Design of the high level software architecture
5. Testing the software, coding and debugging different kind of tasks
6. Design and testing an algorithm for landing on a mobile platform

Chapter 2

Related work

Summary

This chapter synthesizes the preliminary literature review explaining existing research, products and systems. It analyzes some robotics platforms and tools, in particular presents an overview of existing autopilots boards and software as well. A suitable modeling technique for this kind of vehicles is described introducing additional non linearities and explaining when the model uses them. Moreover it introduces a survey on various control techniques that are currently used showing pros and cons. At the end some comments are given about software architecture trends which are used in this field.

2.1 Quadrotor platform

Flying objects have always exerted a great fascination on man encouraging all kinds of research and development. This intrigue for reaching the sky took all the form of imagination such as myths and legends. Many different and bizarre machines were theorized but very interesting were the precursors of the helicopter. Few visionaries, such as Leonardo da Vinci in the late 15th Century, foresaw an aerial application in the widely used windmill (13) coming up with the famous screw design as propeller. Even if it never worked, Leonardo's design was very innovative and this challenge has generated centuries of frustration and hundreds of dramatic attempts without being faded. Only in 1933 Juan de la Cierva gave us the autogiro. The first practical rotocraft invented which led to what we usually call helicopter.

Few years after the first manned plane was invented, Dr. Cooper and Elmer Sperry designed the automatic gyroscopic stabilizer (1), which helps to keep an

2.1 Quadrotor platform

aircraft flying straight and level. This was the kick of unmanned vehicle research which has its starting point back to WWI and WWII. Few years after, sofisticated machines are seen in battle fields such as the famous Predator by General Atom-ics, the Hammeread by Piaggio Aerospace or the Pioneer by Israel Aerospace Industries.



Figure 2.1: Predator Unmanned Aerial Vehicle

In the last ten years technology has taken a giant leap forward and the concept on Micro Aerial Vehicle (MAV) was born. Mavs are a class of UAVs with the feature of being relatively small and may be autonomous. Development is driven by commercial, research, government, and military purpose. The small craft allows remote observation of hazardous environments inaccessible to ground vehicles. MAVs have been built also for hobby purposes, such as aerial robotics contests and aerial photography.

The union of Micro Aerial technology and the helicopter concept brings the quad rotor platform. Quadcopter, also known as quadrotor, is a helicopter with four rotors. The rotors are directed upwards and they are placed in a square formation with equal distance from the center of mass. The quadcopter is controlled by adjusting the angular velocities of the rotors which are spun by electric motors.

Designers came up with different projects and the market is now full of different vendors. The standard platform is the four propeller shape but the architecture can be eventually expanded, with advantages and drawback, up to eight propellers. Those are eventually called octo-copters and they are made to transport heavy load but with very high power consumption. In order to choose the appropriate platform one must examine different models and evaluate which is

2.1 Quadrotor platform

Image	Description	Designer
	Falcon 8 , used by professionals for mapping and inspections.	Produced by Ascending Technologies (8)
	Phantom 3 , ready to use high quality commercial platform.	Produced by DJI (9).
	AR.Drone , ready to fly and cheap.	Produced by Parrot (4).
	Flamewheel , this kit must be assembled by the user. Good quality.	Produced by DJI (9) and assembled by Lorenz Meier (11) from PixHawk team.
	IRIS , almost ready to use. High quality and robust but relatively cheap.	Produced by 3D Robotics (2).

Table 2.1: Some copters designs

the best based on the needs. We can divide copters available on the market in professionals, semi-professional, and not-professional.

Professional copters are often used by qualified people in applications such as film making, inspection, mapping and surveillance. An example is the **Falcon 8** by Asctec, it is very reliable and has fantastic performances. The price however is very high, it is not suitable to fly indoor and the autopilot is not open source. Some Asctec copters are designed for research but the price is too high for our purposes. Semi-professional copters are somewhat a step below the professional segment. Those copter are the most used among amateurs and they are very reliable. The **Phantom 3** is a well known platform, the quality is superb and it comes pre-assembled. Unfortunately the autopilot is not open source and an

additional structure for IR markers must be added since the free surface is pretty tight. Another solution is to build from scratch the platform from a **Flamewheel** frame. In this case every piece is freely chosen, such as motors and autopilot, but the assembling process takes time and may lead to different issues. A very cheap solution is to use an **AR.Drone** by Parrot. It is absolutely ready to fly, the autopilot is not open source even if it supports ROS integration hence we don't have the total control on the robot.

A quadrotor architecture is chosen for this thesis since they are more reliable, suitable for indoor application and more compact in dimensions. IRIS from 3Dr (3D Robotics) is the experimental platform used in this project, it is almost ready to fly and very solid. The autopilot is open source and the price is relatively low. Table 2.1 lists the platform illustrated in this section and a more detailed description of IRIS is given in 3.1.

2.2 Motion capture systems

Motion capture system, or mocap for short, is equipment specialized in the act of recording motion (26) usually through external sensors like cameras. Application of this technology are various and extended in different fields of science and not.

In film making and media industry, mocap systems are used to track the motion of actors in order too translate it in a virtual environment for editing. This simplifies the animation process and enable animators to capture the natural flow of human motion.

Biomechanics is a very promising field and mocap systems plays an important role; researchers and clinicians use motion data to study and observe human performance so they can improve treatment during rehabilitation as well as improve performance in for example sport applications. For example, professional athletes are monitored during the training and with detected motion feedback they can correct their errors in their technique leading to a possible win.

There are many industrial applications areas. From complex 3D vibration applications, vessel tracking above and under water, aerodynamics tests, automotive development, interior design, control design and OEM solutions. The possibility to use motion capture underwater presents completely new possibilities to researchers in many application areas such as ship design, fishing industry and naval research.

Mocaps are widely used in control systems where some feedback is necessary in order to generate some controlling signal, robot performance analysis in particular is a field that widely uses mocap solutions.

This technology is based on cameras able to detect Infra Red (IR) light. Every camera has a LED ring on it which fires IR beams, those beams are hence re-



Figure 2.2: An actor in a motion capture stage, the human movement is copied in a 3d model

flected by passive markers placed in advance on the object we want to observe. The reflected beams are finally detected by cameras and the software is able to reconstruct the position of each marker and the pose of the object.

There are different vendors for this kind of equipment but the most famous are OptiTrack (18) and Vicon (29). They both offer high end technology and high quality solution, the choice just matter of taste and which proprietary software is more suited.

In the setup used in this project, the motion capture system consists in an OptiTrack Flex 13 with 8 cameras.

2.3 Current autopilots

The quadrotor architecture is a pretty old idea, it wasn't take into account for long because people realized that in order to control four motors a decent amount of computing load and battery capacity are needed. However, the recent increase in electronic performances is why quadrotors are so famous right now.

The actual trend is to pack every component in a small amount of space, this idea led producers to design **autopilot boards** with related software.

The most famous board is ArduPilot Mega (7), a professional quality IMU autopilot that is based on the Arduino Mega platform. This autopilot can control fixed-wing aircraft, multi-rotor helicopters, as well as traditional helicopters. It is a full autopilot capable for autonomous stabilisation, way-point based navigation and two way telemetry with Xbee wireless modules. Is very simple to setup with

their own utility hence no programming is required. The ArduPilot Firmware (5) is available on github and its open source under GPLv3 licence. The 'Ardu' part in ArduPilot comes from the fact that originally this software was designed under Arduino environment. Eventually the project outgrew the Arduino platform and they became independent from Arduino run time libraries even if they are still supported. The community is huge, the documentation is very good and recently ArduPilot was used also in important rescue missions becoming the high end solution in commercial and DIY products.

Till now APM seems to be the perfect choice from users stand point, but what about developers? Regarding this aspect some comments are necessary. When a new developer wants to contribute to a project the first thing he does is to check documentation and then experiment a bit with the code. From APM side, the documentation and support are superb, on their website (5) there is everything some could need. The big drawback is the on the technical organization of the code. Since it started from Arduino platform but it evolved quickly, many changes where made. Some files kept the original Arduino extension '*pde*', some kept the famous *.ino* while some other became part of a c library. There is a bit of confusion that could slow down the project, plus the code style is not very modern even if reliable.

On the other hand, IRIS features a PixHawk board (see 3.1.1.1) which by default supports APM but PX4 autopilot can be also installed. PX4(22) is described in 3.1.1.2 and compared to APM has less features and less 'years of experience'. The community is still very active and the project it is growing very fast (24). It has every essential feature for an autopilot, just like APM it can be used on planes, helicopters, multicopters and rovers but the code is very organized and clear. The documentation is enough and a new developer learn pretty fast, this is the main reason IRIS in this project is running PX4 pilot.

2.4 Modeling and control

The derivation of a dynamical model is the starting point for control design; quadrotor modeling was studied and explored extensively in the latest years with different complexity.

Newton-Euler equations are widely used to handle quadrotor modeling as they lead to fairly simple results like in (55) and in (58). A very common practice is to consider the robot as a rigid body, even if it is not true, and treat the aerodynamic propulsion separately. Since inputs of the system are the rates of each propeller, one can define some more realistic inputs calculating the relation of motors speed with force and torques generated (52). Differential inputs are hence used. In

(53) this principle is explained very well, the robot is described with rigid body equations where three torques and one force is applied. Those torques and forces comes right from the propellers thrust, they are the inputs of the system, and namely most of the people calculate them as proportional to the square of each rotor speed. ((35) and (53)).

One may also consider some aerodynamic and additional non linear effects including them in the model and hence increasing accuracy. The simplest improvement could be adding friction with air as form of linear damping, called also drag. A more complex feature to model is called blade flapping (53). In translational flight, the advancing blade of a rotor sees a higher effective velocity relative to the air, while the retreating blade sees a lower effective velocity. This results in a difference in lift between the two rotors, causing the rotor blades to flap up and down once per revolution (47) since they are pretty flexible. The last effect is that the total thrust varies not only with the power input, but with the relative wind velocity, and the angle of attack with respect to the wind. This is further complicated by a flight regime, called vortex ring state, in which there is no analytical solution for thrust, and experimental data shows that the thrust is extremely stochastic.

Those effects are significant in aggressive maneuvering which include sudden change in direction and high speed hence they will not be taken into account.

Controlling such system is a great challenge which arises many issues and proposal by scientific community, hence different controls have been applied to it. The quadrotor does not have complex mechanical control linkages due to the fact that it relies on fixed pitch rotors and uses the variation in motor speed for vehicle control. However, these advantages come at a price as controlling a quadrotor is not easy because of the coupled dynamics and its commonly under-actuated design configuration (31).

The most utilized controllers are:

- PID control
- Linear Quadratic Regulator
- Feedback Linearization
- Sliding Mode Control
- Backstepping Control
- Adaptive Control Algorithms

The **PID controller** has been applied to a broad range of controller applications. It is indeed the most used controller in industry. It is easily tuned even with empirical methods, it has good robustness and it is very easy to implement. It follows that PID is applied also to quadrotors with fairly good results especially in velocity control, attitude control and hovering (53), (42). However PID has some drawbacks due to the non linear nature of the system. Thus a linearization around hovering point is necessary (37) limiting quadrotor performances. Nevertheless PID is implemented most of commercial quadrotors available on the market. Hobbyists and developers fancy so much PID for their platform because it is very simple to tune and it adapts to many structures and geometries. PX4 developers decided to adopt this kind of control in a cascaded fashion to improve adaptability respect to different quadrotor models.

The **LQR optimal control** algorithm operates a dynamic system by minimizing a suitable cost function. Boudallah and co-researchers applied the LQR algorithm to a quadrotor and compared its performance to that of the PID controller (36). LQR is in fact outperforming PID because it is designed on the full non linear system but still it does an average job.

In the field of non linear control, the first technique is **Feedback Linearization**. It relies on putting a non linear system in a special form where it can be treated as linear. It was implemented on a quadrotor platform (30) with good results. Nevertheless, feedback linearization presents an unforgivable drawback. The exact model must be known and this is never the case, in particular among DIY projects.

Sliding mode control is another approach to non linear control. Sliding mode works by applying a discontinuous control signal to the system to command it to slide along a prescribed path thus achieving stability. The main advantages are the good tracking and fact that there is no need to approximate the model dynamics. The discontinuous control signal may cause chattering and power loss. Sliding mode control is often used beside **backstepping** (38) which is a recursive algorithm that breaks down the controller into steps and progressively stabilizes each subsystem. Its advantage is that the algorithm converges fast leading to less computational resources and it can handle disturbances well. The main limitation with the algorithm is its robustness is not good.

More advanced tools are often used such as **Adaptive algorithms**. Adaptive control algorithms are aimed at adapting to parameter changes in the system. The parameters are either uncertain or varying with time and in many cases they were able to control systems where linearization failed. They were proven to be efficient in quadrotor control (32) and the adaptive scheme could lead to many interesting results especially in presence of wind and during pick and place operations of small loads.

2.5 Software architectures and control stations

To conclude this section I would like to point out one important aspect of PID control and why is the selected algorithm for this project. There is a main difference between the presented algorithms, some are model dependent and some others are not. Feedback linearization for example is a very high model-dependent algorithms and same for dynamic canceling. It means that the perfect dynamical model must be known, the parameters well estimated and the dynamics well modeled. As experience teach, this is almost never the case. The PID is not model dependent, the choice of the gains makes it perfectly customizable for many structures and different type of rotor crafts. This is the key aspect on why it is mainly used, especially among amateurs. In fact autopilot boards are sold separately and the user is the one in charge to tune them.

2.5 Software architectures and control stations

A ground control station (GCS) usually is a land or sea-based control center that provides the facilities for human control of unmanned vehicles in the air or in space. A GCS could be used to control unmanned aerial vehicles or rockets within or above the atmosphere. It contains every feature needed to interact with the monitored system such as diagnostics, receive data and send commands, display vehicle state and perform emergency procedures. In some cases a GCS is made by custom hardware depending on the application, they can be mobile or not and have different operational ranges.

For aerial robotics usually the control station consists in a software running on a laptop or tablet and a communication module (radio, wi-fi , bluetooth). Let's have a brief look on which available solutions the market proposes and which is the choice for this project.

Many companies offer proprietary solutions such as **Airware Control Station** (3) but open source solutions are more reachable and expandable. ArduPilot supports **APM Planner** (6) which is the offspring of the well established and mostly used Mission Planner created by Michael Oborne. APM Planner is an open-source ground station application for MAVlink(see 3.1) based autopilots including APM and PX4/Pixhawk that can be run on Windows, Mac OSX, and Linux. The most important features are:

- Point-and-click waypoint entry, using Google Maps
- Download mission log files and analyze them
- Configure APM settings for user airframe
- Interface with a PC flight simulator to create a full hardware-in-the-loop UAV simulator

2.6 Landing on a moving platform

- Calibrate on board sensors
- See vehicle status, parameters and sensors output

It is written using Qt libraries since they have good GUI support and is the first choice among hobbyists and professionals. It can be easily configured to support different vehicles like boats, rovers, helicopters, multicopters and planes.

APM Planner features are shared also by another popular GCS, especially among PX4 users, named **QGroundControl** (25). Additionally to APM Planner, QGroundControl supports multiple vehicle instances at the same time which is essential in swarm robotics. Moreover it has real time sensor plotting, in flight way points manipulation and digital video transmission from on board cameras. QGroundControl is used in this thesis to calibrate IRIS sensors and to tune some parameters.

Those GCSs are clearly designed and optimized for outdoor missions, they have GPS support and displayed maps from Google Earth but position feedback from another source such as a mocap system is not supported. What is lacking is a control station suitable for indoor application and experiments. During this work I designed a software architecture that takes the place of QGroundControl, it is aimed to be used with Optitrack cameras so for lab experiments mainly. The work of this thesis focuses more on the robot management than user experience and interface. It is written in Qt libraries because there could be a future integration with QGroundControl and because they offer many tools with a very good documentation. It sacrifices features such as Point-and-click waypoint entry and sensor calibration and it centralizes the robot performance and in particular robot autonomy. It is responsible of passing the robot position feedback from the mocap taking place of the GPS. The concept of task is presented as an action that IRIS can perform, the software scheduler takes a list of actions created by the user and let the robot execute them autonomously. This architecture is designed to be expanded as much as possible adding new tasks and modes.

The main goal is to go towards a behavioral architecture for quadrotors inspired by an old work by Montgomery James (56) and when the actions are sufficient integrate a planner to replace the user during the task list creation. Autonomy is the key aspect for this software, the idea is abandon the role of the mission operator and switch to a more autonomous system where the human role is just to set a goal.

2.6 Landing on a moving platform

Since many years people studied a way to land aircrafts safely, important studies has been made especially in the field of aerospace exploiting and designing differ-

2.6 Landing on a moving platform

ent techniques to land spacecrafts on other planets. Moreover it happens that the target where the robot wants to land is not still, but performing some kind of motion on the ground. Landing a jet on an air carrier is a perfect example of a moving landing site, the platform is moving and possibly oscillating with waves.

With the arrival of MAVs (Micro Aerial Vehicles) new challenges arise due to their dexterity and small sizes. Usually battery life is very limited and vehicles need to reach automatically recharge stations. A quadrotor may land on a moving car after its mission, on a robot in some cooperation task or on a floating boat to be recovered. All these procedures need a very high precision trajectory tracking and perception of the environment.

Small flying animals are capable of safe and accurate landings while relying only on proprioceptive sensors and visual information. Since this capability holds a promise of landing safely with limited sensors and processing, it has served as inspiration for recent spacecraft landing studies(49). A very interesting research (33) demonstrated how bees, with very simple measurements, are able to land on many surfaces. Dedicated eyes calculate the *optical flow* of images meaning that they are able to track features and estimate the velocity of each feature in image plane. The results of this measurement is a vector field describing how a particular object (feature) in the image plane moves in time or from one frame to another in case of cameras. When I'm going towards a surface with some pattern on it, it is easy to experience an expansion towards the external edges of the image I see of the features (e.g. corners of a pattern). It is easy as well to feel this expansion faster as I am closer to the wall respect when I am far. Keeping this rate of expansion constant, bees are able to land easily. As closer they get to the surface, they measure a higher rate and in consequence they slow down to keep it constant. With this technique bees can safely land assuring that the approaching speed at touchdown is close to zero.

Another useful quantity that can be obtained from the optical flow is the Time To Contact or TTC defined also the ratio of the height and the vertical velocity. From this simple relation some descending control laws are derived (39).

Those methods are developed assuming to have an optical flow sensor or a camera on board pointing downwards. Unfortunately the IRIS does not have those features and we can rely only on the mocap and the IMU for feedback. In this project the position of the platform will be estimated by the motion capture after putting markers on it, this may mimic a localized vehicle sending its position to the quadrotor ensuring the landing maneuver.

The problem is separated in two different aspects, tracking and landing. In order to land tracking must be ensured and the research community proposed different methods. Some used non linear tracking (59) and others, assuming that the

2.6 Landing on a moving platform

velocity of the platform is estimated, compensate the delay of the robot respect to the target with a velocity feed-forward (44). A PI controller is synthesized in (46) closing a velocity control loop while a non linear control law assures the descending task.

Velocity control is not yet implemented in the software architecture and the only reference that is sent is a position set point. Hence I decided to rely only on position control, which may limit the performance of the maneuver but it is simple to implement and it is shown to be a valid strategy.

The idea I followed is to remain as simple as possible avoiding non linear controllers. The experiment with bees, even if very interesting, do not take into account the tracking of a platform which must be integrated. Moreover it shows that bees use a linear law for descending: the vertical velocity decreases linearly with the height from the target. My algorithm is pretty simple but in some sense similar. The height of the IRIS decreases linearly with the horizontal position error respect to the center of the platform. This assures that the tracking has an higher priority respect to the landing which will never occur if the robot is too far away. At the end tracking is made by a PI controller, closed respect the horizontal position error, with an offset. Since we hypothesized that velocity both for the robot and the platform is not available, feedback on position is the best way to solve the task. There are some drawback on using a PI controller such as the overshoot when the platform changes direction but assuming that the motion of the landing site is smooth, the controller is able to secure the landing.

Chapter 3

System description

Summary

This chapter introduces to the reader the current laboratory setup. The first section illustrates which kind of tools are used as well the specifications of each component. The second section instead will present the integration both hardware and software of each part of the system.

3.1 The setup

This section introduces and explains the tools, both hardware and software, that are used in the experiments.

We can identify five distinct parts:

- IRIS quadcopter from 3d robotics
- Motion Capture system from optitrack
- Linux machine
- Windows machine
- Flight arena

While IRIS, the mocap system and the flight arena deserve three separate sections the two machines are described together since they play a central role in the integration part (see [3.2](#)).

3.1.1 IRIS Quadcopter

The IRIS quadcopter is flying robot manufactured by 3D Robotics and commercially available as a kit or ready-to-fly. IRIS flight control system employs by default the open source software ArduPilot running on a Pixhawk autopilot board (based on the PX4 hardware developed by ETH).



Figure 3.1: The IRIS quad copter

The main distinct components of the IRIS quadcopter are the airframe (central body, arms, motors and legs), four 850 kV DC brushless motors controlled in open-loop through PWM, one 11.1 V LiPo battery and control electronics.

The use is mainly commercial, it is optimized for aerial shooting and provides a lot of features the user can play with. IRIS can be easily setup to follow any GPS-enabled Android device with OTG compatibility, this technology controls also the gimbal to keep the camera centered on the target capturing videos and actually becoming a free hand camera. Using the free DroidPlanner app, the user can plan flights by simply drawing a flight plan on any Android tablet or phone. This allows for hands free flight control with virtually unlimited waypoints even keeping IRIS pointing to the same location via a Region of Interest (ROI) waypoint throughout the entire flight (14).

It is easy to understand that this device is designed to fly outdoor, nevertheless it is possible with some software tuning to use the IRIS in indoor scenarios.

3.1 The setup



Figure 3.2: IRIS and control devices.

The component which make this possible is the actual brain of the robot: the PixHawk board with PX4 software. The radio link communications use the MAVlink protocol explained in this section.

3.1.1.1 PixHawk board

PIXHAWK (figure 3.3) is a high-performance autopilot-on-module suitable for fixed wing, multi rotors, helicopters, cars, boats and any other robotic platform that can move. It is targeted towards high-end research, amateur and industry needs and includes all hardware required for remote control (19), stabilization and navigation functions namely:

- an embedded processor (32bit STM32F427 Cortex M4 core with FPU)
- a fail-safe processor (32 bit STM32F103 failsafe co-processor)
- a set of motion sensors, including an Inertial Measurement Unit sensing accelerations and angular speeds of the aircraft, a barometer to compute relative altitude and vertical speed from changes in static air pressure, a magnetometer for compass and a GPS receiver.
- ESCs (Electronic Speed Controllers) that handle low-level motors control loops to maintain required thrust through open-loop PWM control.
- RC Radio to receive direct pilot commands from an RC hand-held controller (2.4 GHz radio link).

3.1 The setup

- telemetry module, a digital radio transceiver (433 MHz) receiving commands from the ground control station and sending telemetry data back to the ground via the *MAVLink* protocol.

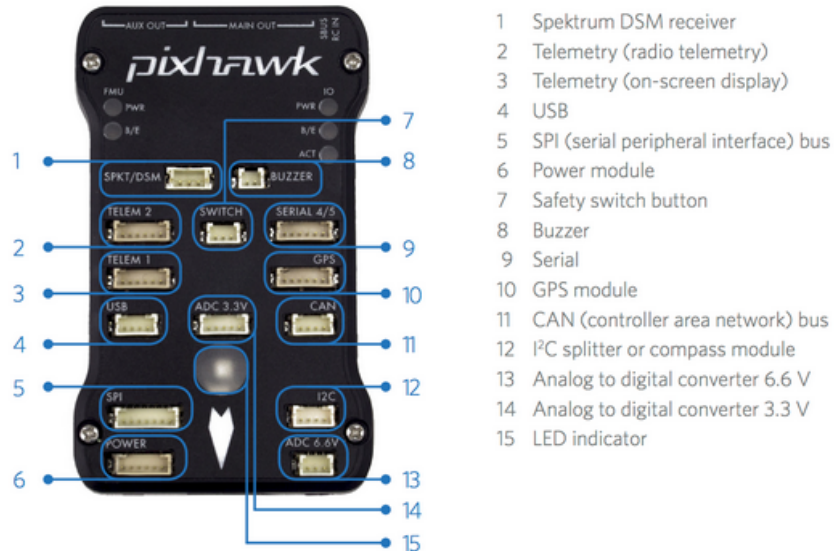


Figure 3.3: Pixhawk board and its connections.

It supports redundant technology both for power and processor, it is equipped with various interfaces such as CAN, SPI, I²C, UART and supports a micro USB for on board real time logging.

3.1.1.2 PX4 Autopilot

PX4 (22) is the software stack running on the autopilot board, it was a master thesis project at ETH pursued by Lorenz Meier and it became a big open source project on github (24) with contributors from all over the world. It works on NuttX (16) which is an open source real time OS and it uses uOrb (micro orb) as middleware. Different modules runs in parallel and they can be grouped in different sets:

- PX4 Flight Stack (estimation and control, cross-platform), the core modules dealing in this thesis
- PX4 Middleware (ORB, NuttX)
- PX4 ESC Firmware (for motor controllers)

3.1 The setup

- PX4 Bootloader (for STM32 boards)
- Operating System (NuttX or Linux/Mac OS)

3.1.1.3 MAVLink Protocol

MAVLink is a very lightweight, header-only message marshalling library for micro air vehicles created and released under LGPL licence by Lorenz Meier in 2009. It can pack, with very little overhead, C-structs over serial channels with high efficiency and send these packets to the ground control station (Fig. 3.4). It is extensively tested on the PX4, PIXHAWK, APM and Parrot AR.Drone platforms and serves there as communication backbone for the MCU/IMU communication as well as for Linux interprocess and ground link communication. It has the possibility to be used with at maximum 255 vehicles on the same control station, it runs on multiple microcontrollers and OS such as ARM7, ATMega, dsPic, STM32 or Windows, Linux, MacOS and iOS with only 8 byte of overhead.

The intense testing of this protocol made it the most used communication protocol in aerial robotics due to his effectiveness.



Figure 3.4: Ground Control Station used to visualize robot parameters, plan missions or calibrate sensors.

Supported data types

MAVLink supports fixed-size integer data types, IEEE 754 single precision floating point numbers, arrays of these data types and the special mavlink version

3.1 The setup

Mavlink supported Data types	
<code>uint8_t</code>	Unsigned 8 bit
<code>int8_t</code>	Signed 8 bit
<code>uint16_t</code>	Unsigned 16 bit
<code>int16_t</code>	Signed 16 bit
<code>uint32_t</code>	Unsigned 32 bit
<code>int32_t</code>	Signed 32 bit
<code>uint64_t</code>	Unsigned 64 bit
<code>uint64_t</code>	Signed 64 bit
<code>char</code>	Characters or strings
<code>float</code>	IEEE 754 single precision floating point number
<code>double</code>	IEEE 754 double precision floating point number
<code>uint8_t mavlink_version]</code>	Unsigned 8 bit field automatically filled on sending with the current MAVLink version - it cannot be written, just read from the packet like a normal <code>uint8_t</code> field

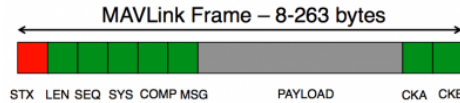
Table 3.1: Mavlink supported data types.

field, which is added automatically by the protocol. Table 3.1 contains a list of every data type that can be transported by mavlink packets (15).

This protocol was designed towards two properties: transmission speed and safety. It allows to check the message content, it also allows to detect lost messages but still only needs six bytes overhead for each packet as illustrated in figure 3.5. Regarding the packets size we have that:

- The minimum packet length is 8 bytes for acknowledge packets without payload
- The maximum packet length is 263 bytes for full payload

3.1 The setup



Byte Index	Content	Value	Explanation
0	Packet start sign	v1.0: 0xFE (v0.9: 0x55)	Indicates the start of a new packet.
1	Payload length	0 - 255	Indicates length of the following payload.
2	Packet sequence	0 - 255	Each component counts up his send sequence. Allows to detect packet loss
3	System ID	1 - 255	ID of the SENDING system. Allows to differentiate different MAVs on the same network.
4	Component ID	0 - 255	ID of the SENDING component. Allows to differentiate different components of the same system, e.g. the IMU and the autopilot.
5	Message ID	0 - 255	ID of the message - the id defines what the payload "means" and how it should be correctly decoded.
6 to (n+6)	Data bytes	(0 - 255) bytes	Data of the message, depends on the message id.
(n+7) to (n+8)	Checksum (low byte, high byte)	ITU X.25/SAE AS-4 hash, excluding packet start sign, so bytes 1..(n+6)	Note: The checksum also includes MAVLINK_CRC_EXTRA (Number computed from message fields. Protects the packet from decoding a different version of the same packet but with different variables).

Figure 3.5: MAVLink package anatomy.

3.1.2 Motion capture system

The localization of the robot in the 3D space relies on the OptiTrack FLEX 13 motion capture system, composed by 8 infrared cameras (Fig. 3.6) mounted on the roof of the laboratory in a squared fashion around the flight perimeter. Is the mid level product in OptitTrack catalogue (1000 dollars per camera (18)) capable of tracking multiple objects in a medium volume space of about 4 X 4 X 4 meters.

3.1.2.1 Image sensor specifications and performances

- Latency: 8.3 ms.
- Frame Rate: 30-120 FPS (adjustable).
- Imager Resolution: 1280 X 1024 (1.3 Megapixels).

3.1 The setup



Figure 3.6: Flex 13 camera and dimensions.

This camera features a status LED and a 2 digits numerical screen for diagnostics, mounting supports, an image sensor and a lens. A 28 LED ring around the lens ensures the required IR (Infra Red) illumination both in stroboscopic and continuous modes.

Object are defined by attaching to them at least 3 **passive infrared markers** (Figure 3.7) able to reflect infrared light, solving rigid bodies and ensure tracking. The number of markers that the OptiTrack is capable of tracking depends on the size of the markers and the distance they are from the camera. This number may change from model to model but is about 100 in our case, more than enough for this project.

The 3D location of markers can be resolved with millimeter accuracy and resolution depending on capture volume size and camera configuration. Increasing the number of cameras can help improve the tracking performance if needed and in this case 0.3 mm of error for each marker is achieved.

3.1.2.2 Software, cameras layout and requirements

The system uses the proprietary software Motive (18), an Optical motion capture software which incorporates many features such as rigid body solving and marker tracking. Motive is able to manage every camera parameter such as exposure, brightness and gain as well as the overall calibration. Two USB hubs divide the eight cameras in two groups collecting four USB cables each coming from each

3.1 The setup



Figure 3.7: Passive IR marker able to reflect IR radiation

sensor. Both hubs are connected through USB cables to the Windows machine where Motive is installed, moreover a sync cable responsible for the synchronization runs from one hub to the other. Figure 3.8 explains the connections of a single hub.

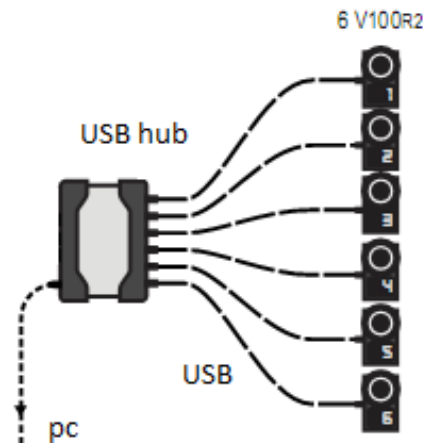


Figure 3.8: Example of a single hub attached to 6 cameras, sync cable between the two hubs is not shown.

The reader must note that in order to have good tracking performances, the setup needs to assure some properties during the experiments:

- At least 3 markers must be present on the object.
- The distance between each marker must be constant during the tracking period (Rigid body assumption).
- Cameras must see at least 3 markers of the tracked rigid body.
- Occlusions are not taken into account by Motive (18).

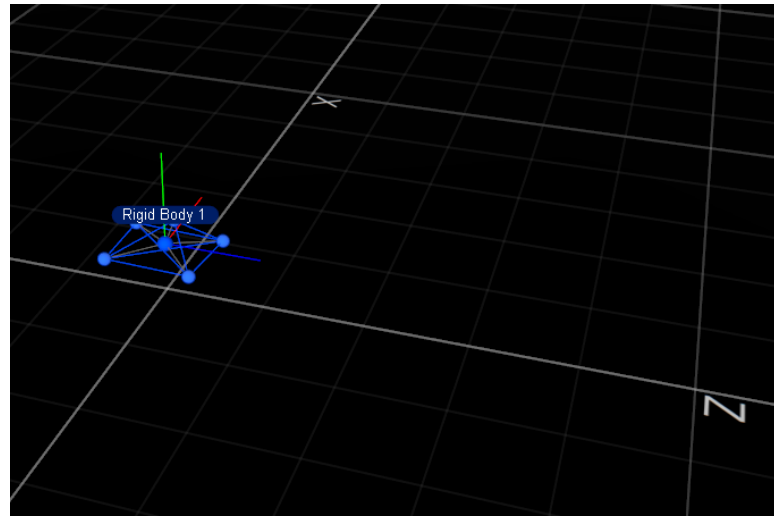


Figure 3.9: IRIS Rigid body created with Motive software.

- Rigid bodies with symmetric shapes induce big uncertainties in attitude estimation.

I solved this problems mainly in two ways. Pointing each camera to the center of the flight space approximately at 0.5 meters from the ground gives the best coverage and few unseen areas at the margins.

Regarding the robot, with 5 markers placed in a 3D asymmetrical configuration on the body frame as in figure 3.10, assures that at least 3 markers are visible always and there are no singularity regarding attitude.

3.1.3 Flight Arena

The flight arena is the stage of the setup. Since the laboratory where this thesis has taken place is new, I was involved in the relocation of the equipment from the old to the new lab. Next I attached every camera to the supports previously drilled one the roof and after I took care of the cables management. Since the maximum allowed length of the camera cables is 5 meters, I managed to place the hubs on the top at two opposite edges of the square (the ones intersecting x axis). By that, the available length is sufficient to connect three cameras of one edge and one from the adjacent edge to on hub and the rest to the other. The sync and the two hubs cables are running on the roof and crossing the room while the camera cables are displaced on the perimeter. Finally I oriented each camera towards the center of the room in order to have the highest coverage possible and calibrated the system. The flying space measures approximately 3 x 3 meters and 1.5 meters high defined by the capture volume of the mocap. Outside there is a

3.2 Overall Integration



Figure 3.10: Markers placed on IRIS in asymmetrical 3D positions.

security perimeter enclosing cameras made by a nylon net of about 4 x 4 meters till the roof. The origin of the position measures is at the center of the room placed on the floor with the z axis going downwards as shown in figure 3.11. A panoramic view of the arena, taken from the top left corner, is shown in figure 3.12.

3.2 Overall Integration

This section explains to the reader how every part of the setup is interfacing with each other, the flow of data packets from OptiTrack to IRIS and the operation done to the information at each step.

3.2.1 Hardware interfaces

Each camera is equipped with a 5 meters USB cable and, as stated in 3.1.2, four cables are connected to one hub and four to the second hub. As outputs, the hubs are equipped with a 5 meter USB cable that can be expanded to 10 meters, those two connection are inputs for the Windows machine.

Windows machine specs

- OS: Windows 7

3.2 Overall Integration

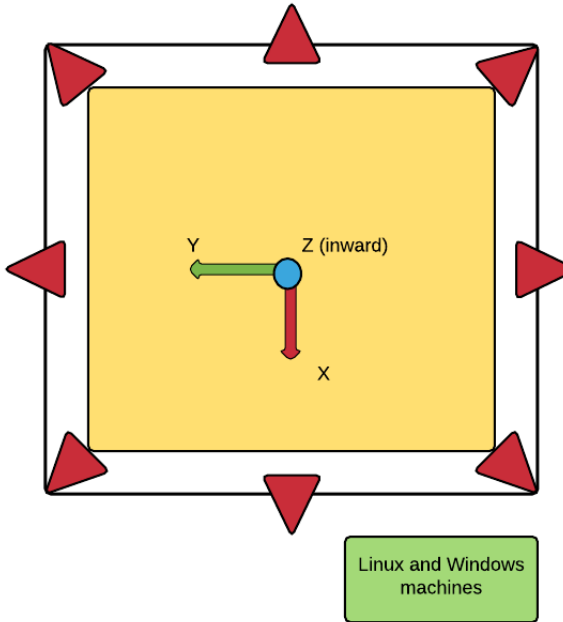


Figure 3.11: A scheme of the flight arena. In red there are the cameras, the yellow part is the flying space while the outer square is the protective net.

- Processor: Intel i7 3.60 GHz
- RAM: 32 Gb
- Video Card: NVIDIA GTX 970
- Software tools: Motive

This computer is directly connected to a Linux machine through Ethernet cable (RJ-45 connectors).

Linux machine specs

- OS: Ubuntu 14.04 LTS
- Processor: Intel i7 2.40 GHz
- RAM: 8Gb
- Video Card: NVIDIA GeForce GTX 760M
- Software tools: Qt C++ Libraries, Px4 build environment ([23](#))

3.2 Overall Integration



Figure 3.12: Panoramic view of the flying space.

At the end, via USB , a telemetry module (Fig. 3.14) is attached to the linux machine. This radio link allows the control station to communicate with the robot wirelessly with acceptable performance. It is mainly used for acquiring telemetry and robot status, transmit new mission goals, check robot parameters such as controller gains and calibrate onboard sensors.

Its main features are (2):

- 433 MHz (for Europe).
- micro usb port: it can be used also from tablets.
- UART Interface.
- 2-way full-duplex communication.
- MAVLink protocol framing.

Moreover, IRIS features a standard RC transmitter, shown in figure 3.2, from which the user can operate the robot in three main modes:

1. Fully manual: radio sticks control directly velocity of the propellers.
2. Semi-auto: height is stabilized, left stick control height position set point while attitude is manual.

3.2 Overall Integration

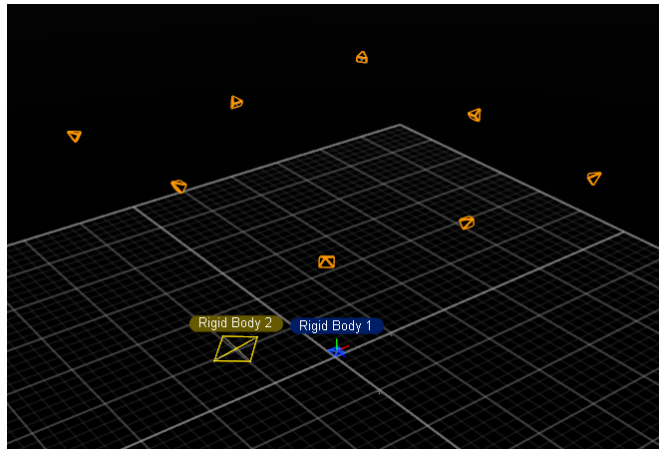


Figure 3.13: Flight arena seen by Motive with a couple of rigid bodies and cameras.

3. Fully-auto: horizontal position is stabilized through position feedback, right stick controls x and y set points.

3.2.2 Software interfaces

Motive has the feature to transmit the pose of every tracked rigid bodies through a multicast IP. By this option, the raw pose of the robot is transmitted to the Linux machine. The software architecture running on Linux reads data coming directly from Motive through a *Receiver component*. Without the use of an *adapter component*, since the program is specific for this application, data from Motive is processed as explained in section 3.2.2.1 at the moment it arrives. In the mean while a position set point is generated inside the architecture, both pose estimation and position set point are packed using MAVLink protocol. At the end data is sent through a socket interface and the telemetry module takes care of transmitting everything to IRIS with a rate of approximately 10Hz.

Figure 3.15 sums up in a scheme the relation between each part.

3.2.2.1 Adapting reference frames

Motive transmits a 6 degree of freedom pose (position and orientation) respect to a fixed reference frame \Re^m in the form:

$$Pose^m = \begin{bmatrix} P^m \\ Q^m \end{bmatrix} \quad (3.1)$$

3.2 Overall Integration



Figure 3.14: Telemetry module from 3d Robotics used to receive and transmit MAVLink Packages with IRIS.

where $P^m = \begin{bmatrix} x \\ y \\ z \end{bmatrix}$ is the position vector and $Q^m = \begin{bmatrix} w \\ x \\ y \\ z \end{bmatrix}$ is the rotation quaternion, everything expressed in Motive reference frame \mathfrak{R}^m .

Now let's define a second reference frame, in this case is a North-East-Down frame (27) mainly used in aeronautics and aerial robotics, namely \mathfrak{R}^E . The peculiarity of this reference is that:

- x axis is aligned with North.
- y axis is aligned with East.
- z axis goes down towards the earth.

The only constraint of \mathfrak{R}^m is that y is vertical and x parallel to the ground, hence x and y can be set freely at the moment of cameras calibration Figure 3.16 shows both reference.

It is easily shown that the relation between frames is a 90 degree rotation of \mathfrak{R}^m over x. Let $R_x(\theta)$ be the rotation matrix on x, P^b arbitrary 3-elements vector column respect to a general base frame b, then the following is valid:

$$(P^m)^T R_x(\theta) = P^E \quad (3.2)$$

3.2 Overall Integration

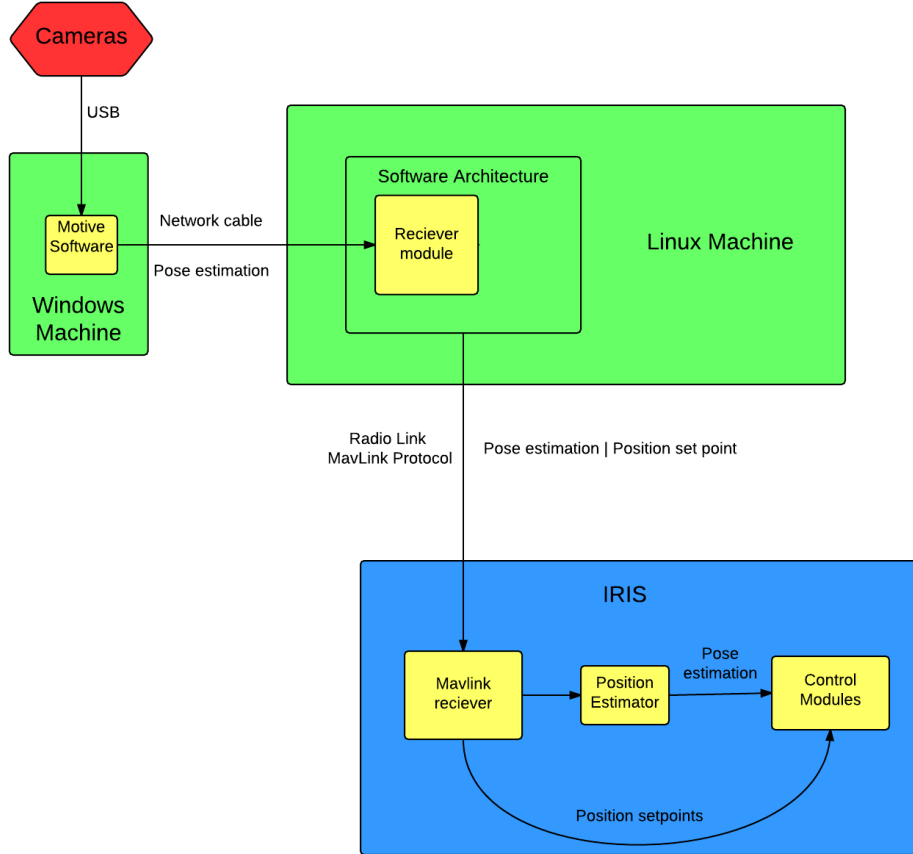


Figure 3.15: Scheme of the setup with connections between parts

$$R_x(\theta) = \begin{bmatrix} 1 & 0 & 0 \\ 0 & \cos(\theta) & -\sin(\theta) \\ 0 & \sin(\theta) & \cos(\theta) \end{bmatrix} \quad (3.3)$$

Putting $\theta = \pi/2$ inside 3.3, then 3.2 become:

$$\begin{bmatrix} x & y & z \end{bmatrix} \begin{bmatrix} 1 & 0 & 0 \\ 0 & 0 & -1 \\ 0 & 1 & 0 \end{bmatrix} = \begin{bmatrix} x \\ z \\ -y \end{bmatrix} \quad (3.4)$$

and

$$P^E = \begin{bmatrix} x \\ z \\ -y \end{bmatrix} \quad (3.5)$$

3.2 Overall Integration

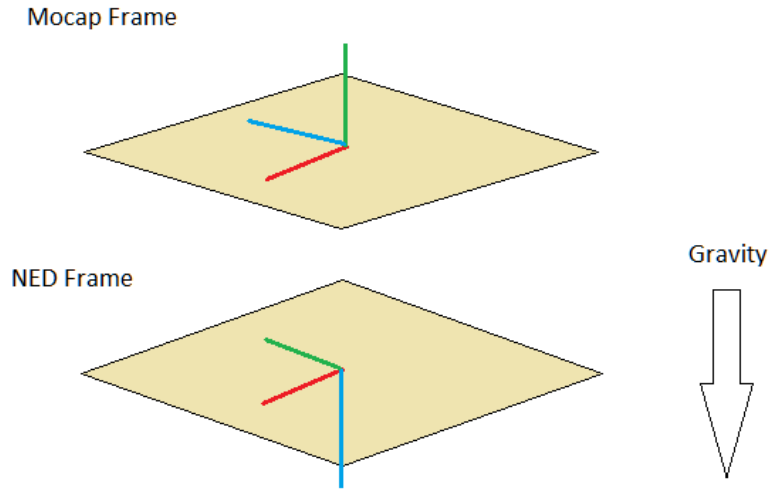


Figure 3.16: NED and Mocap frames depicted. X axis in red, y axis in green and z axis in blue

where $[x, y, z]$ are the coordinates of P^m in \Re^m .

As regards the rotational part, some comments must be done. Since the applied rotation applied does not influence the estimated attitude, we can safely state that:

$$Q^E = \begin{bmatrix} w \\ x \\ z \\ -y \end{bmatrix} \quad (3.6)$$

where $[w, x, y, z]$ are the elements of Q^m .

Equations 3.5 and 3.6 describe the relation between \Re^m and \Re^E in a simple but effective way in fact just by changing the order of the elements of the pose coming out Motive, a pose that IRIS can understand is generated.

Chapter 4

Modeling IRIS

Summary

This part concerns the modeling of the IRIS quad rotor. A model of the quadrotor is necessary to develop a controller and understand better its dynamics. The first part presents some generalities including the reference frames used in order to define the world and the robot. It also contains a list of assumption done to simplify the model. After this are explained the physical principles involved and the actual derivation of the model.

4.1 Generalities

This sections explains general concepts necessary to proceed with modeling. It starts by defining reference frames, then it describes how maneuvering is done and at the end i presents general assumption under which the model is derived.

4.1.1 Reference frames

First element is a world base frame, in section 3.2.2.1 is defined \Re^E which is a North East Down frame with its own features. In our case, the world frame is decided freely after calibration. It is the frame respect to which cameras give the pose estimate. Hence \Re^E still keeps its name being world fixed frame but it has no constraint of being oriented North-East-Down. The only constraint for \Re^E is that ***z axis is directed downwards along gravity while x, y axis are parallel to ground.***

Next frame is the body frame, namely \Re^B . It is attached to the center of mass of the robot with the x axis pointing to the front and z axis downwards, y axis

is generated accordingly with the right hand rule (see fig 4.2+).

The relation between \mathfrak{R}^B and \mathfrak{R}^E is represented by a transformation matrix, namely ET_B which defines the transformation of \mathfrak{R}^B respect to \mathfrak{R}^E as base frame.

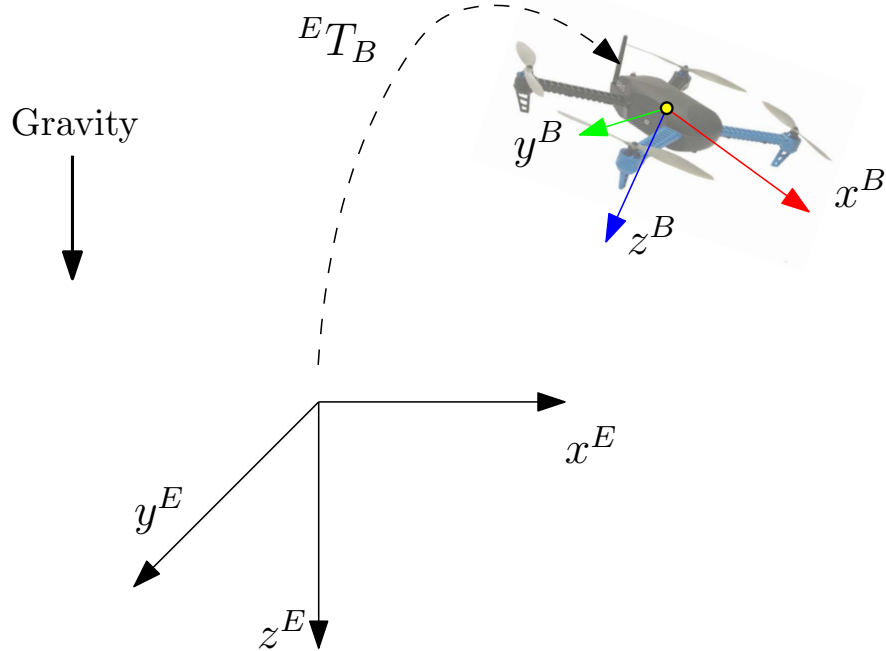


Figure 4.1: Earth-fixed reference frame, body-fixed reference frame and the transformation between them.

4.1.2 General assumptions

The analysis of this system is pretty complex. In order to simplify the derivation of the model some assumption are made and some non linearities are disregarded.

When a rotor translates horizontally through the air, the advancing blade has a higher absolute tip velocity and will generate more lift than the retreating blade. The mismatch in lift generates an overall moment on the rotor disk in the direction of the apparent wind causing the blade to flap as shown in figure 4.2 and the generated thrust is inclined respect to the rotor axis. This effect, called *Blade Flapping* is not included in the derived model.

A second disregarded non linear effect is the *Total Thrust Variation in Translational Flight* (48). The analysis of this phenomenon is quite complex and it is described by a qualitative explanation. When a rotor translates in air, it suffers

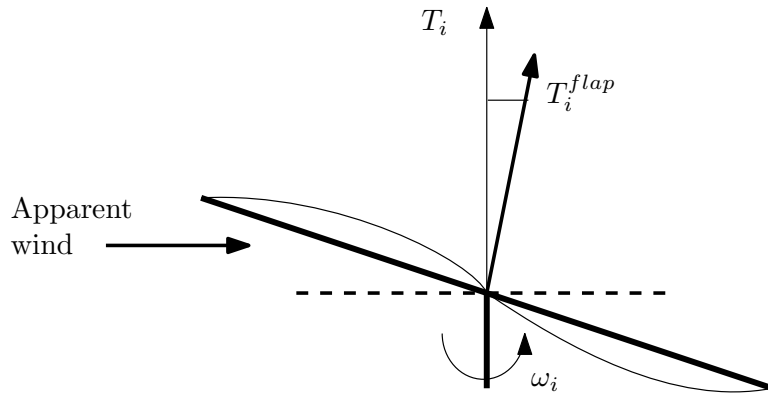


Figure 4.2: Blade flapping effect. T_i is the ideal vertical thrust while T_i^{flap} is the real thrust vector

form apparent wind and an increase of air flux through the blades. This leads to an increase of lift and thrust by the rotor.

Moreover, viscous friction experienced by the robot when it moves is negligible at small velocities. The robot can be also considered as a rigid body since there are no significant strains and forces applied which may deform the structure.

To summarize, the following assumption are made:

- Blade Flapping is not considered
- Thrust Variation in Translational Flight is disregarded
- Viscous friction (drag) is neglected
- The robot is considered as a rigid body
- Motor dynamics are managed internally by the board and not included in the model

4.2 Transformation matrices

This introduces some mathematical tools necessary to develop a full dynamical model for the quadrotor system. Moreover I will present here the conventions used for representing angles and rotations and the derivation of the matrices involved.

4.2 Transformation matrices

In section 4.1.1 I introduced ${}^E T_B$ as the transformation matrix of \Re^B with respect to \Re^E . In particular ${}^E T_B$ is a 4x4 matrix and has a fixed structure (51):

$${}^E T_B = \begin{bmatrix} {}^E R_B & {}^E P_B \\ O_3^T & 1 \end{bmatrix} \quad (4.1)$$

in this definition we can see three different terms. ${}^E R_B$ is the rotation matrix of frame \Re^B with respect to \Re^E ; ${}^E P_B = \begin{bmatrix} x \\ y \\ z \end{bmatrix}$ is the position of the center of mass of the robot respect to the Earth frame and $O_3 = \begin{bmatrix} 0 \\ 0 \\ 0 \end{bmatrix}$.

Rotation matrix and angles

Every rotation in 3D space can be defined by 3 successive rotations about 3 principal axis; we can define separately each rotation matrix about each axis and then multiply them.

Each Right-Hand rotation about a particular axis is defined by a positive angle (34) from earth to body frame and the following definitions are true:

$$R_x(\phi) = \begin{bmatrix} 1 & 0 & 0 \\ 0 & \cos(\theta) & \sin(\theta) \\ 0 & -\sin(\theta) & \cos(\theta) \end{bmatrix} \quad (4.2)$$

$$R_y(\theta) = \begin{bmatrix} \cos(\theta) & 0 & \sin(\theta) \\ 0 & 1 & 0 \\ -\sin(\theta) & 0 & \cos(\theta) \end{bmatrix} \quad (4.3)$$

$$R_z(\psi) = \begin{bmatrix} \cos(\psi) & -\sin(\psi) & 0 \\ \sin(\psi) & \cos(\psi) & 0 \\ 0 & 0 & 1 \end{bmatrix} \quad (4.4)$$

The general rotation matrix can be obtained by multiplying elementary rotations, but please note that the order is important.

The most common sequence associated with the name *Euler angles* is (z, x, z) or ${}^E R_B = R_z(\phi)R_x(\theta)R_z(\psi)$.

There is however a more suitable sequence which fits our case. The angles associated with the sequence (x, y, z) are sometimes called *Cardan angles* or *Tait-Bryan*

4.3 Propulsion and controls

angles. Commonly used in aerospace where ϕ , θ , and ψ are known respectively as **roll**, **pitch**, and **yaw**. These angles describe a vehicle whose forward direction is along the positive body-fixed x-axis and the body-fixed z axis downward, like in the case of the quadrotor (see 4.1.1). In such configuration, the home position $\begin{bmatrix} \phi \\ \theta \\ \psi \end{bmatrix} = \begin{bmatrix} 0 \\ 0 \\ 0 \end{bmatrix}$, is flat and level pointing forward along the world x axis. The non intuitive downward pointing z axis is chosen in order to make a positive change in θ correspond to pitching upward (41).

That said, the multiplication order used is (x, y, z) . Developing the calculations, the general rotation matrix becomes:

$${}^E R_B = R_x(\phi)R_y(\theta)R_z(\psi) = \begin{bmatrix} c_\theta c_\psi & s_\phi s_\theta c_\psi - c_\phi s_\psi & c_\phi s_\theta c_\psi + s_\phi c_\psi \\ c_\theta s_\psi & s_\phi s_\theta s_\psi + c_\phi c_\psi & c_\phi s_\theta s_\psi - s_\phi c_\psi \\ -s_\theta & c_\theta s_\phi & c_\theta c_\phi \end{bmatrix} \quad (4.5)$$

where $c = \cos$ and $s = \sin$ for simplicity. Moreover, the following limits are true by definition:

- $-\pi < \phi < \pi$
- $-\pi/2 < \theta < \pi/2$
- $-\pi < \psi < \pi$

while the following shows the transformation from the derivative of the Euler angles to the angular velocity in the body frame(44):

$$W = \begin{bmatrix} 1 & 0 & -s_\theta \\ 0 & c_\phi & c_\theta s_\phi \\ 0 & -s_\phi & c_\theta c_\phi \end{bmatrix} \quad (4.6)$$

Please also note that ${}^E R_B$ is an orthonormal 3x3 matrix so its inverse it is equal to its transpose (51), hence $({}^E R_B)^{-1} = ({}^E R_B)^T = {}^B R_E$.

4.3 Propulsion and controls

The four motors installed are responsible of the propulsion of the quadcopter. Each rotor-motor couple rotates with an angular velocity ω_i and generates: an upward lifting force f_i parallel to the body z axis z^B and a reaction torque τ_r . This quantities approximated by a linear model where:

$$f_i = k\omega_i^2 \quad (4.7)$$

4.3 Propulsion and controls

$$\tau_i = k_d \omega_i^2 \quad (4.8)$$

k and k_d are positive constants depending on atmospheric conditions and blade geometry. These constants can be identified through dynamical tests.

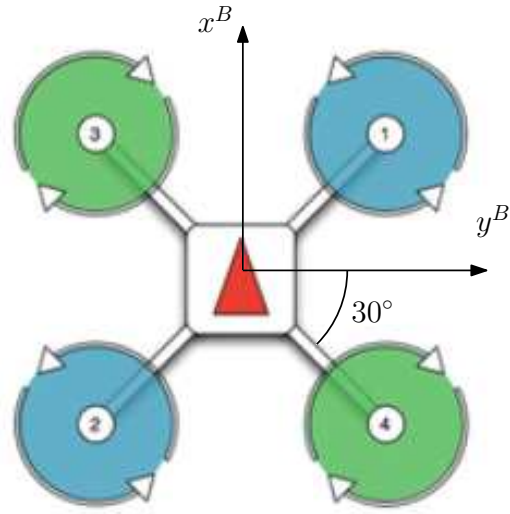


Figure 4.3: Motor labeling and spinning

The total thrust T acting on the robot's center of mass, parallel to z^B and directed upwards is:

$$\mathbf{T}^B = \begin{bmatrix} 0 \\ 0 \\ \sum_{i=1}^4 f_i \end{bmatrix} \quad (4.9)$$

while the total moments

$$\tau_\phi = \sum_{i=1}^4 d_i \sin(\alpha_i) f_i \quad (4.10)$$

$$\tau_\theta = - \sum_{i=1}^4 d_i \cos(\alpha_i) f_i \quad (4.11)$$

$$\tau_\psi = \sum_{i=1}^4 \sigma_i \cos(\alpha_i) \tau_i \quad (4.12)$$

where f_i and k are defined in 4.7; τ_i and k_d in 4.8; d_i is the distance from the center of the rotor to the center of mass; σ_i is positive if ω_i is positive and negative

4.3 Propulsion and controls

otherwise; α_i is the angle between the vector going from the center of mass to the i -th motor and y^B (30° for IRIS).

By rearranging 4.10, 4.11 and 4.12 in matrix form:

$$\begin{bmatrix} T^B \\ \tau_\phi \\ \tau_\theta \\ \tau_\psi \end{bmatrix} = \begin{bmatrix} k & k & k & k \\ kd_i \sin(30) & -kd_i \sin(30)k & -d_i \sin(30) & d_i \sin(30) \\ -kd_i \cos(30) & -kd_i \cos(30)k & d_i \cos(30) & d_i \cos(30) \\ k_d & -k_d & -k_d & k_d \end{bmatrix} \begin{bmatrix} \omega_1^2 \\ \omega_2^2 \\ \omega_3^2 \\ \omega_4^2 \end{bmatrix} \quad (4.13)$$

$$\begin{bmatrix} T^B \\ \tau_\phi \\ \tau_\theta \\ \tau_\psi \end{bmatrix} = H \begin{bmatrix} \omega_1^2 \\ \omega_2^2 \\ \omega_3^2 \\ \omega_4^2 \end{bmatrix} \quad (4.14)$$

where in this case T^B is the value of the force directed through z^B , τ_ϕ is the torque along x^B , τ_θ is the torque along y^B and finally τ_ψ is the torque along z^B . The force T^B is responsible of the translation or the body frame while the three torques generate rotations in each principal axis.

Figure 4.3 shows how motors are labeled in IRIS and the respective direction of rotation while 4.4 is a diagram with the applied forces on the rigid body.

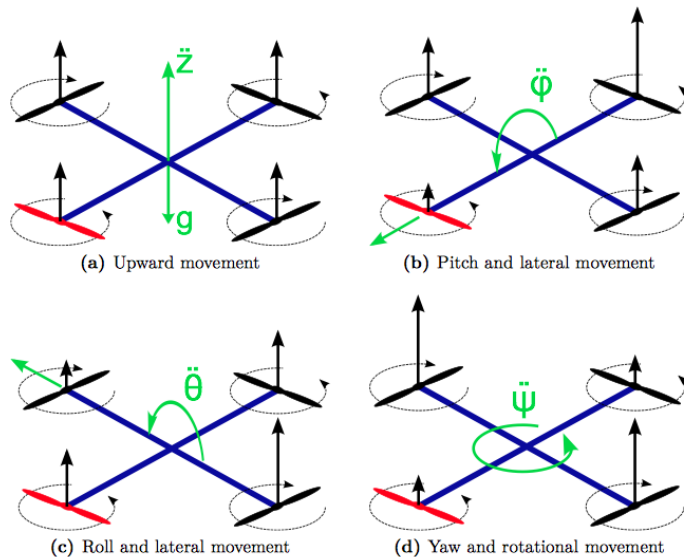


Figure 4.4: Dynamics of the copter. Assume that x axis points towards the red propeller for simplicity, black arrows are the generated forces f_i from aerodynamics. Green arrows represent forces and torques generated combining the rotational speed of the propellers.

4.4 Complete model

Equation 4.13 shows the relation between the squared velocity of each rotor and the generated force and torques . Hence the problem can be split in two parts, aerodynamics and equations of motion. Therefore, **the model is defined as a rigid body on which one external force T^B and three external torques $[\tau_\phi; \tau_\theta; \tau_\psi]$ are applied.** Those external perturbations are calculated in 4.3 and they correspond to the aerodynamic propulsion of the blades.

4.4.1 Rigid body equations

In order to develop the full dynamical model, the control signals must be introduced. Let us define U as a 4-element control vector, then the following is true by definition:

$$\mathbf{U} = \begin{bmatrix} T^B \\ \tau_\phi \\ \tau_\theta \\ \tau_\psi \end{bmatrix} \quad (4.15)$$

Let us also approximate the inertia of the blades equal to zero for simplicity as in (58). We can define the following quantities:

- $\mathbf{r} = \begin{bmatrix} x \\ y \\ z \end{bmatrix}$ position of the robot in Earth frame.
- $\boldsymbol{\eta} = \begin{bmatrix} \phi \\ \theta \\ \psi \end{bmatrix}$ attitude of the quadcopter respect to earth frame (roll, pitch, yaw) presented in 4.2.
- $\boldsymbol{\Omega} = \begin{bmatrix} p \\ q \\ r \end{bmatrix}$ body angular speed respect to each axis in body frame.
- ${}^E R_B = R(\boldsymbol{\eta})$ rotation matrix encoding body attitude defined in 4.2 such that $\mathbf{x}^E = R(\boldsymbol{\eta})\mathbf{x}^B$.
- $W = W(\boldsymbol{\eta})$ Euler angle rate matrix defined in 4.2 relating $\boldsymbol{\Omega}$ with $\dot{\boldsymbol{\eta}}$

The dynamics of the quadcopter can be described by the use of Newton-Euler cardinal equation for motion of a general 6 DOF rigid body suffering from an external force and torque. The four equations for the undergoing motion are defined as the following:

$$\dot{\mathbf{r}} = \mathbf{v} \quad (4.16)$$

$$m\dot{\mathbf{v}} = \mathbf{F} \quad (4.17)$$

$$\dot{\mathbf{R}} = R\Omega_x \quad (4.18)$$

$$I\dot{\boldsymbol{\Omega}} = -\boldsymbol{\Omega} \times I\boldsymbol{\Omega} + \boldsymbol{\tau} \quad (4.19)$$

where the vector \mathbf{F} is the resultant of all the external forces applied on the rigid body's center of mass and $\boldsymbol{\tau}$ is the total torque acting on the body. Ω_x is a 3x3 skew symmetric matrix such that $\Omega_x \mathbf{v} = \boldsymbol{\Omega} \times \mathbf{v}$ for the vector cross product \times and any vector \mathbf{v} (53). The matrix $I = \begin{bmatrix} I_{xx} & 0 & 0 \\ 0 & I_{yy} & 0 \\ 0 & 0 & I_{zz} \end{bmatrix}$ is a diagonal inertia matrix due to the symmetries of the body about principal axis while m is the total mass of the robot.

Equations for translation Since viscosity in air is not considered, the total forces acting on the robot are the gravity mg and the thrust generated by the rotors \mathbf{T}^B calculated in equation 4.9.

Let us define $U_1 = T^B$ meaning the first element of the control vector U introduced in 4.15 where T^B is the module of the thrust directed along z^B (see equation 4.13). As consequence (4.17) can be written as follows:

$$\dot{\mathbf{v}} = \frac{1}{m} \left(\begin{bmatrix} 0 \\ 0 \\ mg \end{bmatrix}^E + R \begin{bmatrix} 0 \\ 0 \\ U_1 \end{bmatrix}^B \right) \quad (4.20)$$

Note: the first column vector in equation 4.20 is the gravity force and is directed along z^E on its positive direction (downwards). The second column vector is the thrust in body frame which is along z^B pointing to its positive direction. The multiplication with the rotation matrix R rotates the thrust vector expressing in earth frame since \mathbf{v} must be expressed in earth frame.

Equations for rotation The total torques acting on the robot are those originated by the commanding maneuvers calculated in equation 4.13 and the gyroscopic effect induced by the rotating blades.

The gyroscopic torques can be neglected because the mass of the blades is very low, then the total torque applied on the rigid body is the one originated

by the lifting forces and we have that $\boldsymbol{\tau} = \begin{bmatrix} \tau_\phi \\ \tau_\theta \\ \tau_\psi \end{bmatrix}$. Those values are namely the second, the third and the forth elements of the control vector U hence equation 4.19 becomes:

$$\dot{\boldsymbol{\Omega}} = I^{-1} \left(\begin{bmatrix} U_2 \\ U_2 \\ U_4 \end{bmatrix} - \boldsymbol{\Omega} \times I\boldsymbol{\Omega} \right) \quad (4.21)$$

where it assumes this simple form due to the assumption of null gyroscopic effects.

Moreover, equation 4.18 can be substituted by the explicit relation between angle rates in earth and in body frame through the matrix W (50). Thus, equation 4.18 is replaced by:

$$\dot{\boldsymbol{\eta}} = W\boldsymbol{\Omega} \quad (4.22)$$

where, for recalling, $\boldsymbol{\Omega}$ is the angular velocity vector in body frame.

Full non linear model

Expanding equations 4.16, 4.20, 4.22 and 4.21 we obtain the full mathematical model represented by the following differential equations:

$$\left\{ \begin{array}{l} \dot{x} = v_x \\ \dot{y} = v_y \\ \dot{z} = v_z \\ v_x = -\frac{U_1}{m}(\cos(\phi) \sin(\theta) \cos(\psi) + \sin(\phi) \sin(\psi)) \\ v_y = -\frac{U_1}{m}(\cos(\phi) \sin(\theta) \sin(\psi) + \sin(\phi) \cos(\psi)) \\ v_z = g - \frac{U_1}{m}(\cos(\phi) \cos(\theta)) \\ \dot{\phi} = p - r \sin(\theta) \\ \dot{\theta} = q \cos(\phi) + r \cos(\theta) \sin(\phi) \\ \dot{\psi} = r \cos(\phi) \cos(\theta) - q \sin(\phi) \\ \dot{p} = \frac{1}{I_{xx}}(U_2 + qr(I_{yy} - I_{zz})) \\ \dot{q} = \frac{1}{I_{yy}}(U_3 + pr(I_{zz} - I_{xx})) \\ \dot{r} = \frac{1}{I_{zz}}(U_4 + pq(I_{xx} - I_{yy})) \end{array} \right. \quad (4.23)$$

I want to stress that this model does not take into account factors such as aerodynamic drag, ground effect, blade-flapping, gyroscopic effects or advanced aerodynamics phenomena. Even with these approximations, this model is the most used in the research because it assures good precision.

Simplified model

Further simplifications can be applied, let us consider the quadrotor in the flat position and now assume that the variation of roll and pitch angles are reasonably small. This is a logical assumption since the quadcopter is designed to fly around such configuration; we can assume that $\phi \approx 0$ and $\theta \approx 0$ and the matrix W becomes an identity matrix as consequence. Therefore under those conditions we have that $\dot{\eta} = \Omega$ and the model is:

4.4 Complete model

$$\left\{ \begin{array}{l} \dot{x} = v_x \\ \dot{y} = v_y \\ \dot{z} = v_z \\ \dot{v}_x = -\frac{U_1}{m}(\cos(\phi) \sin(\theta) \cos(\psi) + \sin(\phi) \sin(\psi)) \\ \dot{v}_y = -\frac{U_1}{m}(\cos(\phi) \sin(\theta) \sin(\psi) + \sin(\phi) \cos(\psi)) \\ \dot{v}_z = g - \frac{U_1}{m}(\cos(\phi) \cos(\theta)) \\ \dot{\phi} = p \\ \dot{\theta} = q \\ \dot{\psi} = r \\ \dot{p} = \frac{U_2}{I_{xx}} \\ \dot{q} = \frac{U_3}{I_{yy}} \\ \dot{r} = \frac{U_4}{I_{zz}} \end{array} \right. \quad (4.24)$$

Please note that only the rotational dynamics are simplified. This model, even with the various assumptions and the linearization, is often used to try simple control algorithm and design linear controllers. In our case it is useful since this project do not include the study on aggressive maneuvering or high velocity motions, the small angle variation for roll and pitch is a valid assumption in fact thi model is used to design controllers for hovering.

m	total mass of the robot	1.308 Kg
I_{xx}	inertia for the x axis	0.0018 Kg m^2
I_{yy}	inertia for the y axis	0.0012 Kg m^2
I_{zz}	inertia for the z axis	0.0027 Kg m^2
k	thrust coefficient	0.1
k_d	drag coefficient	0.1

Table 4.1: IRIS parameters. The moment of inertia are taken from the autopilot parameters file while the aerodynamic coefficients are taken from the blade technical sheet

Chapter 5

Control and state estimation

Summary

Due to the nature of the dynamics of the quadrotor, several control algorithms have been applied to it. As to be expected, each control scheme has its advantages and disadvantages. This chapter presents the techniques that are used to estimate the system's states and to stabilize IRIS which are currently implemented in the PX4 Firmware.

After a quick overview of the estimator modules, the controller architecture is presented. Moreover, this chapter explains in details how the on board autopilot interfaces with the software architecture and which modules are involved.

5.1 Introduction to the PX4 Flight Stack

The PX4 Flight Stack denotes the list of all the applications running on board the PixHawk. Those modules provide the services and methods which are necessary to manage the radio communications, inter process message pass-through, data logging, state estimation, control, high level states and low level communication with motors and sensors.

5.1.1 Message pass-through

The core on board applications are started at system startup, others can be started via the NuttShell or forced to startup by inserting them in the start boot file. Every application runs independently with its own frequency; the interfaces between processes are managed by *uOrb* middleware (Micro Orb) which, with the use of topics, guarantees the message pass-through for data packets over named buses. Those topics encode structs and they are pre defined. In PX4, a

5.1 Introduction to the PX4 Flight Stack

topic (often called node) contains only one message type, e.g. the *vehicle attitude* topic transports a message containing the attitude struct (roll, pitch and yaw estimates).

Nodes can publish a message on a bus/topic or subscribe to a bus/topic. They are not aware of who they are communicating with. There can be multiple publishers and multiple subscribers to a topic (Figure 5.1). This design pattern prevents locking issues and is very common in robotics. **To make this efficient, there is always only one message on the bus and no queue is kept (28)**. The total list of *uOrb* topics can be found in the *uOrb* folder of the PX4 Firmware since the online documentation is not updated.

The external communication (through radio link) is managed by mavlink, previously presented in section 3.1.1.3, however Mav packets are translated in uOrb topics internally.

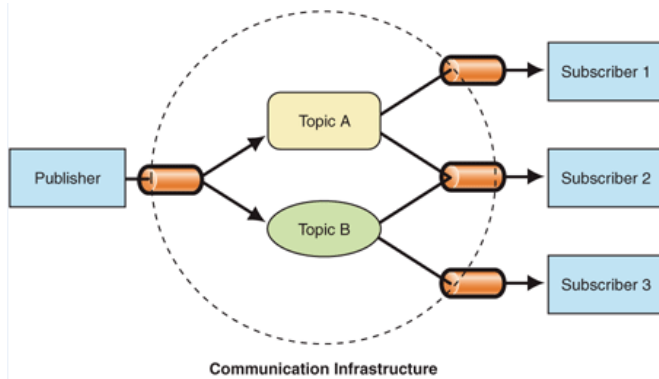


Figure 5.1: Publish/Subscribe design pattern.

5.1.2 Onboard nodes

The most relevant apps that are started at boot can be divided in groups.

System applications Those kind of nodes manage the internal and external process communications , logging and testing. They provide the basic services on which the other modules rely:

- mavlink - is dedicated to pack and unpack mavlink messages.
- sdlog2 - takes relevant topics and creates a log file on sd card at every flight.

5.1 Introduction to the PX4 Flight Stack

- test - mainly used for troubleshooting.
- uOrb - inter-process communication middleware .

Drivers As one may imagine, those nodes represent the layer between hardware and software. They manage the communication with sensors, ports and buses:

- esc_calib - calibration of the electronic speed controllers for motors.
- fmu - manages the board input and output pins.
- GPS - GPS receiver driver
- pwm - command the pwm to be sent to motor controllers
- sensor - communication with various sensors (inertial, baro)

Attitude and position estimators Those modules are responsible for position and attitude estimation, they are part of the core of the flight stack:

- position_estimator_inav - estimates position with inertial sensor, gps and mocap measurements.
- att_estimator_ekf - estimates attitude using inertial sensors.

Multirotor Attitude and Position Controllers Those are the key modules regarding this thesis. They implements the algorithms for position and attitude control:

- mc_pos_control - position controller
- mc_att_control - attitude controller

Flight safety and navigation Those are the key modules regarding this thesis. They implements the algorithms for position and attitude control:

- commander - internal state machine which determine system states for safety (flying, idle , emergency , on ground)
- navigator - highest level of abstraction, it implements mission following and failsafe

5.1.3 State machine overview

The system relies on a state machine in order to manage what it can and cannot do at a particular moment. The main task of this module is to assure safety from an high level point of view. Other safety procedures are implemented also on a lower level on hardware.

The main states are *ARMED*, *STAND-BY*, *INIT*, *ERROR* and *UNLOCKED*. At the moment the user turns on the robot, the state machine is in *INIT* state. Here all the procedure for sensor initialization and checklists are done. The next state then becomes *STAND-BY* where IRIS waits for orders. By manually pressing a safety button, the state changes to *UNLOCKED* and back to *STAND-BY* by pressing again the button. In *UNLOCKED* state, the motor are electrically connected to the power source thus they can be armed. With a button on the remote control, the motors are armed and start spinning with idle velocity and the robot can fly. From any state, an error signal may arrive changing the actual configuration to *ERROR*. Here the motors are turned off after the automatic landing procedure and the robot must be rebooted. Those concept are depicted in figure 5.2.

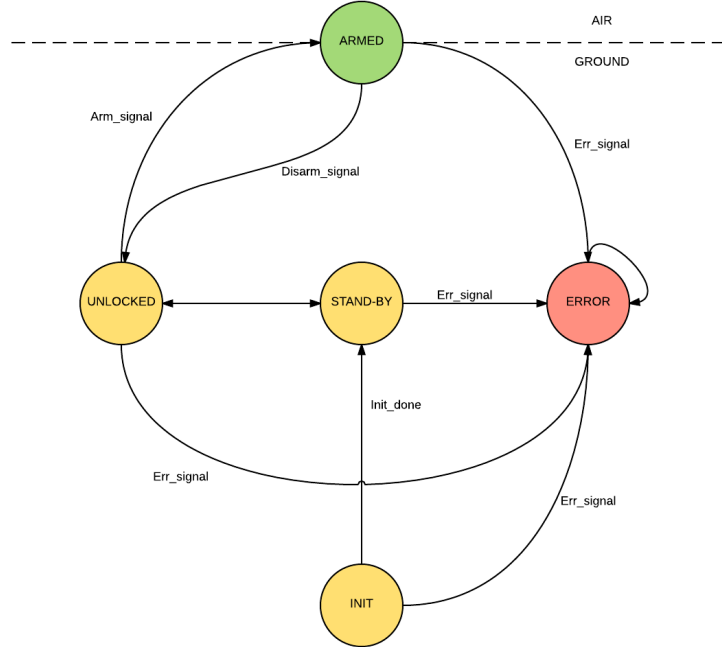


Figure 5.2: IRIS state machine

5.2 Estimation modules

Since I am using an older version of PX4 because it is stable and well tested, the estimation occurs in two different modules. The first module, called *position_estimator_inav*, is used to estimate the position of the quadcopter while the second, named *att_estimator_ekf*, estimates the attitude. The choice of dividing in two different processes the estimation phase is mainly because attitude has an higher dynamics than position, this gives the possibility to run the attitude estimator at a frequency higher than the position estimator thus having better results.

5.2.1 Position estimator

The position estimator is based on inertial model and optimized for multirotors. It reads multiple sensors and estimates 3D position and velocity, in local and global frames. It is a fixed gain estimator and it relies on the following sources with the respective gains:

Sensor	ID	Gain
Accelerometer (for altitude)	Used as an absolute measure	-
Barometer (gives absolute altitude)	INAV_W_Z_BARO	0.0001
Accelerometer (for x and y)	Used as an absolute measure	-
GPS altitude	INAV_W_Z_GPS_P	0.005
GPS Position	INAV_W_XY_GPS_P	1
GPS Velocity	INAV_W_XY_GPS_V	2
GPS climb rate	INAV_W_Z_GPS_V	2
Mocap estimate (altitude)	INAV_W_Z_VIS_P	5
Mocap estimate (altitude)	INAV_W_XY_VIS_P	7

Table 5.1: Correction gains and available measures

Note: the accelerometers are used as an absolute measure, thus treated as the input of the system used for prediction (equation 5.1). Moreover I changed the gain *INAV_W_Z_BARO* from 50 to 0.0001 because the sensor gives the absolute altitude above sea level while the mocap gives the height respect to the earth frame (the floor of the room). This causes a mismatch in the two measures leading to false prediction with a constant offset, hence the gain for the barometer is set very low.

Working principle of position estimator

The algorithm for position estimation is divided in two phases: prediction and update. The model used for **prediction** is the following:

$$\begin{aligned}\mathbf{x}_k(\mathbf{x}_{k-1}, dt, \mathbf{a}) &= \mathbf{x}_{k-1} + \mathbf{v}_k dt + \frac{1}{2} \mathbf{a} dt^2 \\ \mathbf{v}_k(\mathbf{v}_{k-1}, \mathbf{a}, dt) &= \mathbf{v}_{k-1} + \mathbf{a} dt\end{aligned}\tag{5.1}$$

where the vector \mathbf{x}_k encodes the position in earth frame, the vector a represent the acceleration in each axis given by the accelerometer, v_k is the vector of velocities and dt is the time different between the steo k and $k - 1$.

In compact form the we can write the system as the following:

$$\begin{aligned}\mathbf{F}_k(\mathbf{x}_{k-1}, dt, \mathbf{v}_{k-1}, \mathbf{a}) &= \begin{bmatrix} \mathbf{x}_k \\ \mathbf{v}_k \end{bmatrix} \\ \mathbf{y}_k &= H \mathbf{F}_k\end{aligned}\tag{5.2}$$

where \mathbf{y}_k is the output (from sensors) and the H matrix relates the state with the measurements.

Equation 5.2 is usually called **prediction**. It means that with the last available estimate of $[\mathbf{x}_{k-1}, \mathbf{v}_{k-1}]$ and the actual value of the acceleration \mathbf{a} (input of the model) given by the accelerometers, we can predict what could be the next value for \mathbf{F}_k and by consequence the output vector \mathbf{y}_k .

The last item is the **correction** or the calculation of the actual estimated value for the state. The correction equation takes the following form:

$$\mathbf{F}_k^{est} = \mathbf{F}_k^p(\mathbf{x}_{k-1}, dt, \mathbf{v}_{k-1}, \mathbf{a}) + L(\mathbf{y}_k - \mathbf{y}_k^p)\tag{5.3}$$

meaning that the estimated (corrected) state \mathbf{F}_k^{est} is equal to the **prediction** calculated in equation 5.2 (the superscript p stands for prediction) plus the **innovation** $L(\mathbf{y}_k - \mathbf{y}_k^p)$. The innovation term is composed by L which is a diagonal matrix with the values of the correction gains listed in table 5.1 for each sensor and the difference of the **actual measure read by the sensor**, namely \mathbf{y}_k , with the predicted output \mathbf{y}_k^p calculated in 5.2.

At the end the results are published on *vehicle_local_position* topic.

5.2.2 Attitude estimator

Attitude estimation is a bit more complex being a faster dynamics and accurate results are needed. This module relies on an extended Kalman filter, which is the

5.2 Estimation modules

non linear version of the very famous linear quadratic estimator. The model is of the form:

$$\begin{aligned} \mathbf{x}_{k+1} &= \mathbf{f}(\mathbf{x}_k, \mathbf{u}_k) + \boldsymbol{\xi}_k \\ \mathbf{y}_k &= \mathbf{g}(\mathbf{x}_k) + \boldsymbol{\eta}_k \end{aligned} \quad (5.4)$$

where $[\boldsymbol{\xi}_k \sim N(0, Q), \boldsymbol{\eta}_k \sim N(0, R)]$ are gaussian noises on the system and on the measurements with zero mean and $[Q, R]$ covariances. The available sensors used are:

- magnetometer - for calculating magnetic field on the three robot axis (in robot frame).
- gyroscope - for the calculation of angular rates in body frame (p,q,r).
- accelerometer - for retrieving the value of the acceleration (e.g estimation of the vertical through gravity).

The model used is the rotational part of the system 4.23 (last six equations) with the angular accelerations plus the three value of the magnetic field given by the magnetometer. A well detailed description of the algorithm for this particular case is given in (10).

Yaw estimation The lab environment presented a couple of issues regarding the measure of the magnetic field. Being indoor, with electronic equipments and with electrical cables passing under the floor, the magnetic field is not constant along the room volume. This causes bad estimates for the yaw. Being yaw dynamics pretty slow with respect to roll and pitch, we can estimate it off board with a simple trick.

Let $\mathbf{mag}^B = \begin{bmatrix} mag_x \\ mag_y \\ mag_z \end{bmatrix}$ the magnetic field vector in body frame given by the magnetometer and fed to the attitude estimator. Since the earth magnetic field is inclined by almost 30 degrees downwards and pointing north, we can fake it and decide ourself where the north is. Hence let $\mathbf{mag}^E = \begin{bmatrix} 1 \\ 0 \\ 0.4 \end{bmatrix}$ meaning that x^E

becomes the north. The attitude estimator accepts the magnetometer output in body frame hence the "fake" value we provide, by hacking in the module source file, becomes:

$$\mathbf{mag}^B = {}^B R_E \mathbf{mag}^E \quad (5.5)$$

where ${}^B R_E$ is the transpose of R which depends on attitude angles. Roll and Pitch are estimated on board but the yaw is obtained by the mocap measure,

thus we can construct the rotation matrix and calculate the rotated magnetic field in body frame. This approach works, is simple and gives us the possibility to choose where the north(yaw = 0) is without having the problem of alignment of x^E with the North-South line.

5.3 Controller architecture

As stated in chapter 2, those modules implement PIDs controller. The architecture is in the form of what is called a cascaded structure, a very common practice in control design for flying vehicles.

The basic idea is to break up the dynamics of the quadrotor and face the problem piece by piece (54). Thus, the design is divided in four sub controllers placed in a cascaded fashion one after the other. Each controller generates the input for the next one and takes the output of the previous. From the highest to the lowest level we have: *position control*, *velocity control*, *attitude control* and *motor control*. In the context of this thesis, dynamics of motor control are not analyzed but just a brief overview is given.

The **position controller** calculates the velocities set points in the three directions which are fed to the velocity controller. The task of the **velocity controller** is to track those set points by generating attitude reference signals and total thrust. The desired angular pose is tracked by the **attitude controller** which generates the desired torques as input of the **mixer**. The role of the mixer is to calculate each rotor angular speed in order to track the desired signal. This is simply done by inverting equation 4.14 and expressing the angular speed vector in function of the input vector U obtaining:

$$H^{-1} \begin{bmatrix} T^B \\ \tau_\phi \\ \tau_\theta \\ \tau_\psi \end{bmatrix} = \begin{bmatrix} \omega_1^2 \\ \omega_2^2 \\ \omega_3^2 \\ \omega_4^2 \end{bmatrix} \quad (5.6)$$

where the left hand side vector is the output of the attitude (for torques) and position (for thrust) controllers while the right hand side vector is the square of the desired rotor angular speeds. The matrix H is the mixer matrix, it is specific for the robot configurations and it is usually given as a parameter file from the quadcopter designer. At the end of the chain there is the motor controller which, through PWM, assures the convergence to the desired spinning velocity.

Note that those controllers run at different rates, from the position controller which has the lowest rate to the attitude controller which have the highest. Moreover the following assumption is made: **in the chain, one controller converges**

5.3 Controller architecture

faster than its previous one. This is necessary otherwise the cascade will not work properly. Those concepts are represented in figure 5.3.

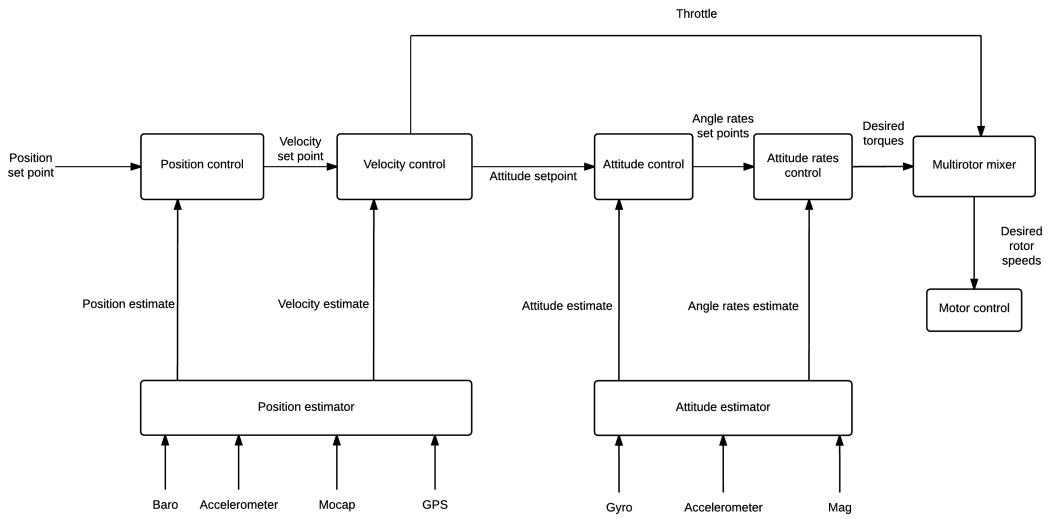


Figure 5.3: Controller overall structure.

For the IRIS, three main modes are available:

- manual - the signals from the radio command are fed directly into the mixer
- altitude stabilized - throttle signal is calculated by the controller in order to track an altitude set point given by the user with the radio command. Attitude is still manual.
- position stabilized - the full position set point, **given by the software architecture**, is tracked by the controller chain.

Note: in position stabilized usually the set point is given by the radio command, I changed the autopilot in order to bypass the radio and send set points with the software architecture. Altitude stabilized is used for emergency since one can easily switch mode with a button on the radio.

5.3.1 Position controller

The position control is straightforward. First the position error is calculated with the feedback from the inertial estimator

$$e_p = \mathbf{pos}_{sp} - \mathbf{pos} \quad (5.7)$$

and then the desired velocity vector is generated with a proportional control law having:

$$\mathbf{vel}_{sp} = K_p \mathbf{e}_p \quad (5.8)$$

where $K_p = 1$ is the proportional gain. \mathbf{pos} , \mathbf{pos}_{sp} and \mathbf{v}_{sp} are 3-elements vectors and they represent respectively the actual robot position in earth frame, the position target set by the software architecture and the generated velocity setpoint.

5.3.2 Velocity controller

Velocity control occurs in two stages. First a desired thrust vector is calculated with a PID control law and then the desired attitude is generated from the thrust vector. The velocity error is defined as:

$$\mathbf{e}_v = \mathbf{vel}_{sp} - \mathbf{vel} \quad (5.9)$$

and the desired thrust vector in earth frame

$$\mathbf{th}_{sp} = K_p^{vel} \mathbf{e}_v + K_d^{vel} \dot{\mathbf{e}}_v + K_i^{vel} \int \mathbf{e}_v \quad (5.10)$$

with $[K_p^{vel}, K_d^{vel}, K_i^{vel}] = [0, 0, 0]$ and gains are diagonal matrices with the values for x y and z in order to be able to set different gains for different dynamics. At this point we can calculate attitude set points, in the form of rotation matrix to avoid singularities, from thrust vector. The desired z axis of the robot is

$$\mathbf{z}_{des}^B = -\frac{\mathbf{th}_{sp}}{\|\mathbf{th}_{sp}\|} \quad (5.11)$$

since the thrust vector points up and z down. Next, from the yaw value ψ given by the attitude estimator, we calculate the intermediate vector for axis y in XY plane

$$\mathbf{y}_c = [-\sin(\psi), \cos(\psi), 0]^T \quad (5.12)$$

and then with the cross product the desired robot x axis is calculated

$$\mathbf{x}_{des}^B = \mathbf{y}_c \times \mathbf{z}_{des}^B \quad (5.13)$$

As consequence the desired robot y axis is

$$\mathbf{y}_{des}^B = \mathbf{z}_{des}^B \times \mathbf{x}_{des}^B \quad (5.14)$$

The desired rotation matrix, ready to be sent to the attitude controller is

$$\mathbf{R}_{des} = [\mathbf{x}_{des}^B \quad \mathbf{y}_{des}^B \quad \mathbf{z}_{des}^B] \quad (5.15)$$

where $[x_{des}^B, y_{des}^B, z_{des}^B]$ are 3-dimensional column vectors expressed in earth frame denoting the desired axis of the body.

Finally the total thrust U_1 is calculated, the first element of the input vector which is directly sent to the mixer is

$$U_1 = \|\mathbf{th}_{sp}\| \quad (5.16)$$

5.3.3 Attitude controller

In order to calculate the last three element of the input vector \mathbf{U} , the attitude controller takes place. First thing to do is to define the rotation error between

the desired rotation matrix and the actual one. Let $S = \begin{bmatrix} 0 & -c & b \\ c & 0 & -a \\ -b & a & 0 \end{bmatrix}$ be a general skew-symmetric matrix, the following is true

$$S^\wedge = \begin{bmatrix} a \\ b \\ c \end{bmatrix} \quad (5.17)$$

and the operator \wedge is called vee map. Then we can define the error vector as the following:

$$\mathbf{e}_r = \frac{1}{2}(R_{des}^T R - R^T R_{des})^\wedge \quad (5.18)$$

Next, similarly to the position controller, we introduce the desired angular rater in body frame as

$$\Omega_{des}^B = K_p^{rot} \mathbf{e}_r \quad (5.19)$$

and right after the angular rate error is

$$\mathbf{e}_\omega = \Omega_{des}^B - \Omega^B \quad (5.20)$$

with Ω^B and R given by the attitude estimator. Finally, through PIDs controller, the command torques are generated and:

$$\begin{bmatrix} U_2 \\ U_3 \\ U_4 \end{bmatrix} = K_p^\omega \mathbf{e}_\omega + K_d^\omega \dot{\mathbf{e}}_\omega + K_i^\omega \int \mathbf{e}_\omega \quad (5.21)$$

where the gains are diagonal matrices with the value of the gain of each dynamics (roll, pitch and yaw rates).

5.4 Results and validation

Some preliminary tests were done in order to evaluate the performances of the controller and the estimator modules. The results are presented in plots taken from the on board logging module and then visualized with FlightPlot , an open source tool available on PixHawk website ([12](#)).

5.4.1 Estimator validation

The validation of the estimation is the first test made before flying. The robot was turned on and moved around the room by hands with the motors unarmed for safety. The on board estimation of the attitude is then compared with the vision estimate from the mocap.

Roll estimation The estimation for the roll is very good. The vision signal is delayed respect to the on board estimation due to the radio link delay. In this particular experiment, at second 15, the robot orientation was lost for a moment by the cameras probably because of an occlusion. At that moment a spike appears and it is visible on the plot in figure [5.4](#).

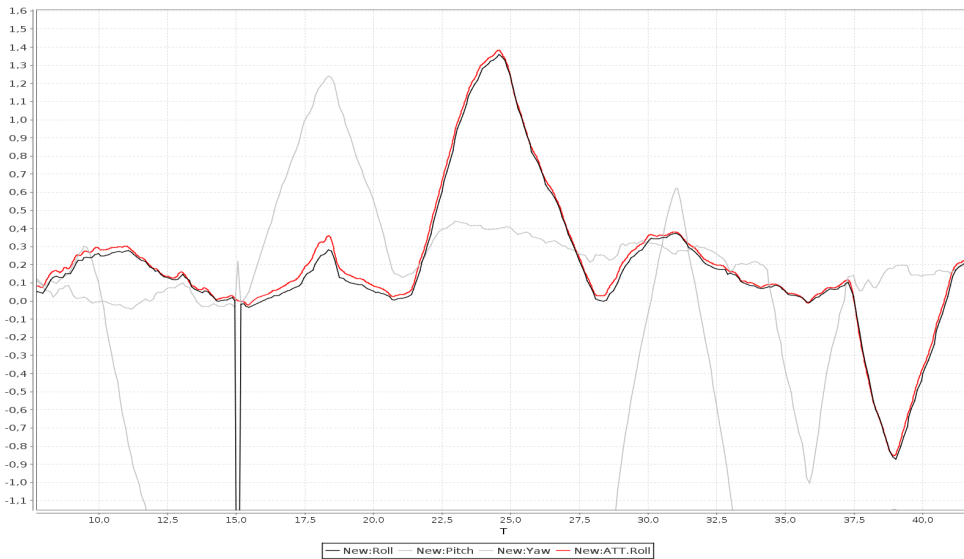


Figure 5.4: Estimation for the roll angle. In black the mocap value while in red the estimated value. Roll is measured in radians.

5.4 Results and validation

Pitch estimation [5.5](#) As for roll, the estimation of the pitch is consistent. Similar spike appears after 15 seconds (figure [5.5](#)).

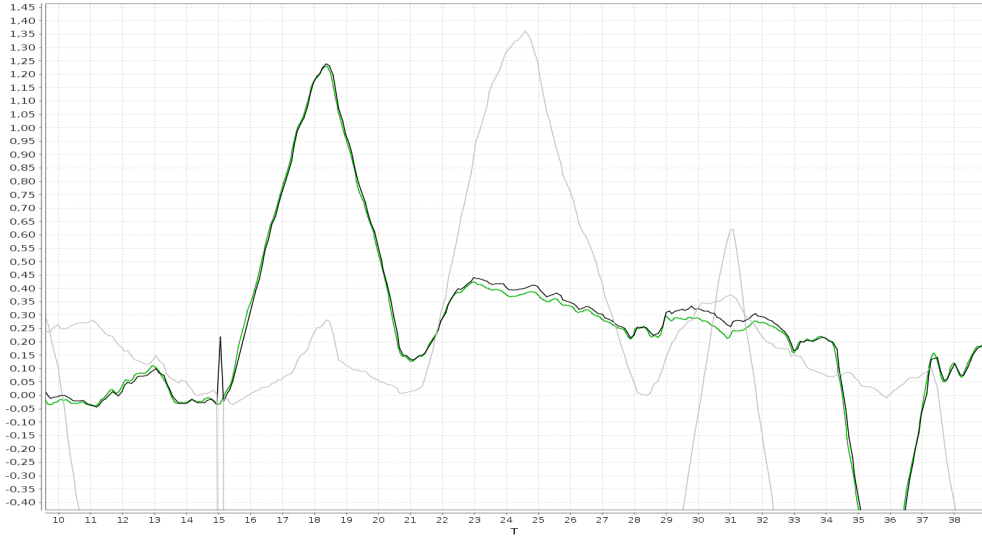


Figure 5.5: Estimation for the pitch angle. In black the mocap value while in green the estimated value. Pitch is measured in radians.

Yaw estimation The yaw estimation is nearly perfect (see figure [5.6](#)). It does not present the same delay as for roll and pitch because it relies mostly on the mocap feedback. After 43 seconds a jump appears because angle abruptly changed from $-\pi$ to π . However this does not affect the robot dynamics because internal computations are done with rotation matrix representation(see section [5.3.3](#)).

5.4 Results and validation

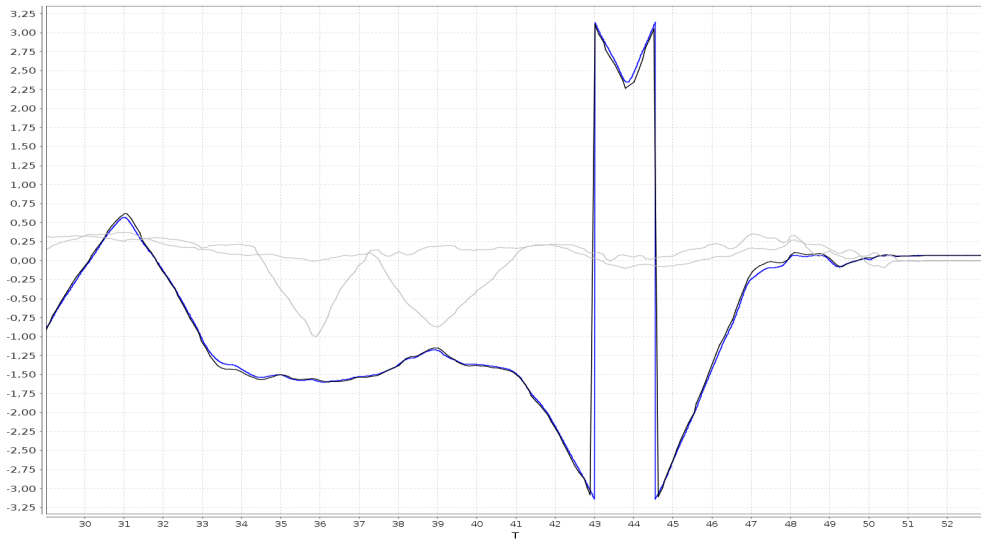


Figure 5.6: Estimation for the yaw angle. In black the mocap value while in blue the estimated value. Yaw is measured in radians.

Position estimation results are not shown because they are optimal and the two curves are perfectly superimposed.

5.4.2 Controller results

The preliminary test, in order to evaluate the controller performances, is to send to the robot position set points in a square wave fashion. In other words, the robot executes a square trajectory with the vertices at: [0.7, -0.7] ; [0.7, 0.7] ; [-0.7, 0.7] ; [0.7, 0.7].

The plots for the position and the yaw are presented since they are the most relevant.

X and Y position The performance over the horizontal plane is decent. Oscillations are mainly induced by the wind generated by the rotors, bouncing on the walls and back to the robot. See Figure 5.7, 5.8.

5.4 Results and validation



Figure 5.7: Convergence on x. The red plot is the robot position while the black is the set point. Position is measured in meters.

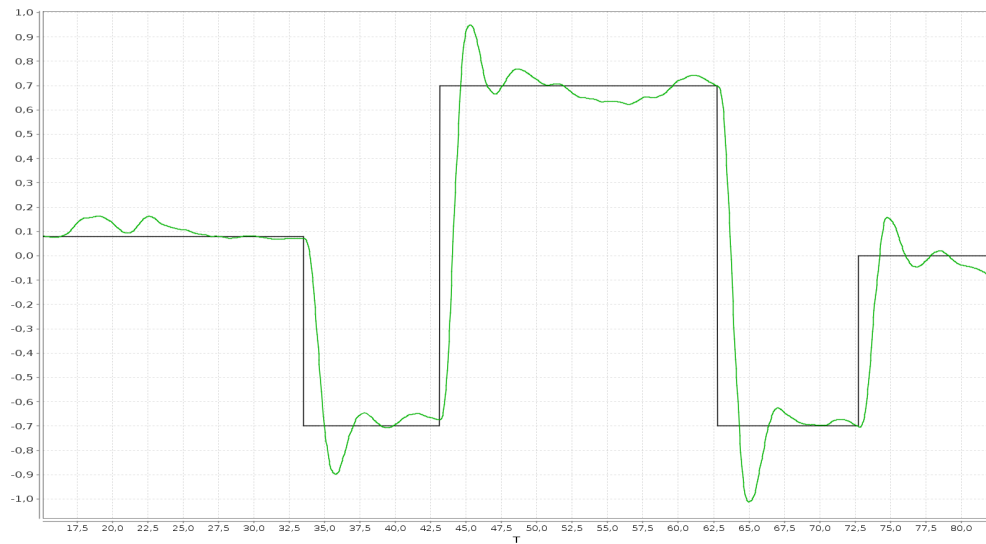


Figure 5.8: Convergence on y. The green plot is the robot position while the black is the set point. Position is measured in meters.

The maximum error is about 10 centimeter in hovering. The overshoot recalls a second order system response

5.4 Results and validation

Z position The z converges more slowly when the robot starts (see figure 5.9), this is because the integrator in the desired thrust vector needs to be saturated. By putting as initial condition of the integrator the value of the gravity force one can avoid this problem, which appears only at the beginning during flight. After 70 seconds the landing maneuver starts.

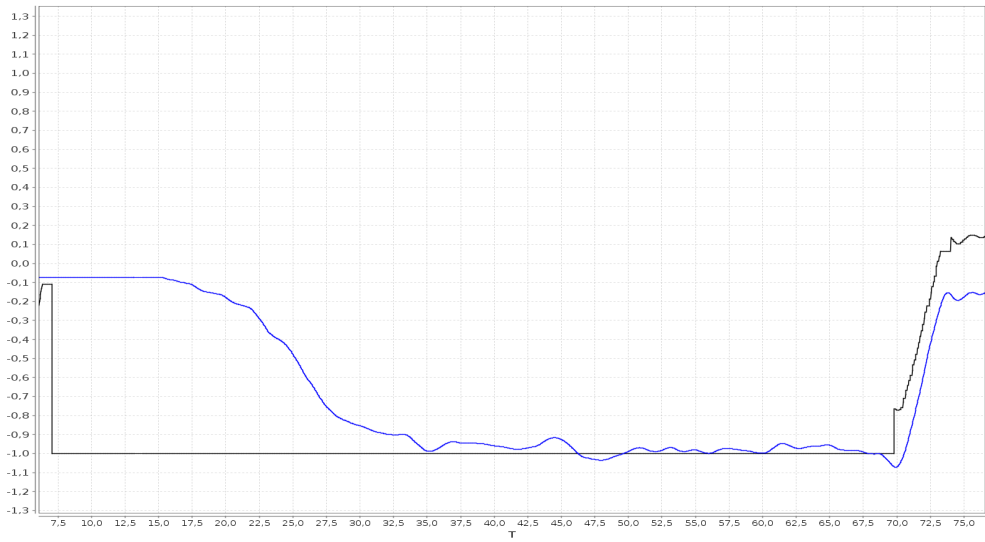


Figure 5.9: Convergence on z. The blue plot is the robot position while the black is the set point. Position is measured in meters. Note that with negative z the robot goes actually up.

Yaw convergence The yaw is commanded by sending yaw set points in a ramp fashion. The ramp appears segmented to the robot since the sending frequency is much lower than the processing rate on the board. In this particular experiment, the robot is asked to look at a specific point. The software architecture send to the robot a desired point (x, y) on the horizontal plane, the robot calculates the yaw needed to face at that particular location and then the controller tracks it. Two different points were chosen, that is why we have two ramps (see figure 5.10).

5.4 Results and validation

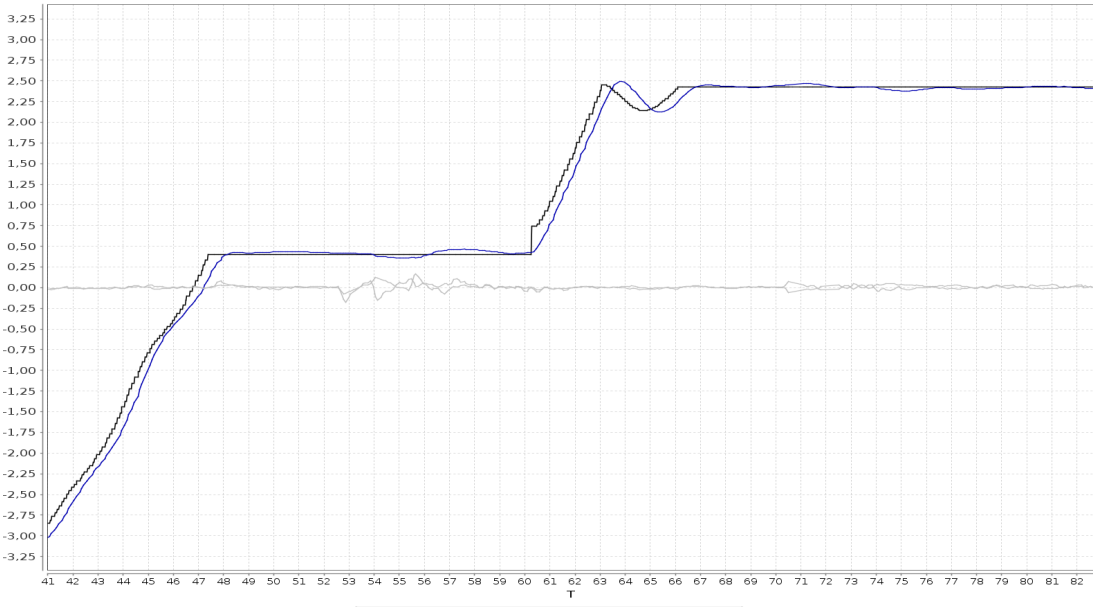


Figure 5.10: Yaw set point tracking, the blue is the real value while the black is the set point

Hovering with disturbances The last experiment consists in asking the robot to hover (stay still) on a point and perturbing it by pushing and pulling with a stick. Thus an external disturbing force, which is represented by arrows in figure figure 5.11, is applied.

5.4 Results and validation



Figure 5.11: Static hover with external perturbations. Red plot is x , green is y and blue is z . The horizontal set point is at $(0, 0)$ and the height is variable. Light blue represent the set point on z .

Chapter 6

Software architecture

Summary

This chapter introduces the reader to the software architecture running off board on Linux. The introduction presents a general overview on software architectures, expressed the needs of such a system and in particular it describes the environment and software tools involved. Next section presents the design pattern according to which the software is organized explaining its advantages and limitations. Then the software components are described with more detail one by one and the results of the experiments are reported.

- 6.1 Introduction to the proposed architecture**
- 6.2 Design patterns**
- 6.3 Software description**
- 6.4 Experiments and results**

Chapter 7

Landing on a mobile platform

Summary

Chapter 8

Results

Summary

Chapter 9

Conclusions

Write the conclusions here...

Appendix A

Extra

Write here...

References

- [1] Gyroscopic stabilizer. The Sperry Gyroscopic Stabilizer, 1915. published on Flight magazine, available on <http://www.flightglobal.com/pdfarchive/view/1915/>. 4
- [2] 3D Robotics store. <https://store.3drobotics.com/products>, 2015. Accessed: 16-08-2015. 6, 28
- [3] Airware control station. <http://www.airware.com/products/ground-control-software>, 2015. Accessed: 18-08-2015. 12
- [4] ARDrone website. <http://ardrone2.parrot.com/>, 2015. Accessed: 18-08-2015. 6
- [5] Ardupilot Firmware. <http://ardupilot.com/>, 2015. Accessed: 16-08-2015. 9
- [6] ArduPilot Mission Planner. <http://planner2.ardupilot.com/>, 2015. Accessed: 18-08-2015. 12
- [7] Ardupilot website. <http://www.ardupilot.co.uk/>, 2015. Accessed: 16-08-2015. 8
- [8] Ascending Technologies. <http://www.asctec.de/en/>, 2015. Accessed: 18-08-2015. 6
- [9] DJI website. <http://www.dji.com>, 2015. Accessed: 15-08-2015. 6
- [10] Extended Kalman Filter for the PX4 autopilot. https://pixhawk.org/firmware/apps/attitude_estimator_ekf, 2015. Accessed: 16-08-2015. 51
- [11] Flamewheel built by Lorenz Meier. https://pixhawk.org/platforms/multicopters/dji_flamewheel_450, 2015. Accessed: 19-08-2015. 6

REFERENCES

- [12] FlightPlot visualizaion tool. <https://pixhawk.org/dev/flightplot>, 2015. Accessed: 18-08-2015. 56
- [13] Helicopter hisorical website. <http://www.helicopter-history.org/>, 2015. Accessed: 20-08-2015. 4
- [14] IRIS, 3d Robotics. <https://store.3drobotics.com/products/iris>, 2015. Accessed: 15-08-2015. 17
- [15] MAVLink protocol description. <http://qgroundcontrol.org/mavlink/start>, 2015. Accessed: 15-08-2015. 21
- [16] NuttX website. <http://nuttx.org/>, 2015. Accessed: 16-08-2015. 19
- [17] Optihub image. http://www.fontysvr.nl/mediawiki/index.php/OptiTrack_FLEX:V100R2, 2015. Accessed: 15-08-2015.
- [18] OptiTrack website. <http://www.optitrack.com/>, 2015. Accessed: 15-08-2015. 8, 22, 23, 24
- [19] PixHawk board description. <https://pixhawk.org/modules/pixhawk>, 2015. Accessed: 15-08-2015. 18
- [20] PixHawk project at ETH. <https://pixhawk.ethz.ch/>, 2015. Accessed: 19-08-2015.
- [21] Predator image. <http://www.airforce-technology.com/projects/predator-uav/predator-uav6.html>, 2015. Accessed: 20-08-2015.
- [22] PX4 autopilot description. https://pixhawk.org/firmware/source_code, 2015. Accessed: 15-08-2015. 9, 19
- [23] PX4 build environment. https://pixhawk.org/dev/toolchain_installation_lin, 2015. Accessed: 16-08-2015. 27
- [24] PX4 Firmware Github. <https://github.com/PX4/Firmware>, 2015. Accessed: 16-08-2015. 9, 19
- [25] QGroundControl website. <http://qgroundcontrol.org/>, 2015. Accessed: 19-08-2015. 13
- [26] qualisys website. <http://www.qualisys.com/>, 2015. Accessed: 16-08-2015. 7
- [27] Reference frames. https://pixhawk.org/dev/know-how/frames_of_reference, 2015. Accessed: 16-08-2015. 30

REFERENCES

- [28] uOrb user guide. https://pixhawk.org/dev/shared_object_communication, 2015. Accessed: 18-08-2015. 46
- [29] Vicon website. <http://www.vicon.com/>, 2015. Accessed: 18-08-2015. 8
- [30] E. Altug, J. Ostrowski, and R. Mahony. Control of a quadrotor helicopter using visual feedback. *Proceedings of IEEE International Conference on Robotics and Automation*, 1, 2002. 11
- [31] S. J. Andrew Zulu. A Review of Control Algorithms for Autonomous Quadrotors. *Open Journal of Applied Sciences*, pages 547–556, 2014. 10
- [32] G. Antonelli, E. Cataldi, P. R. Giordano, S. Chiaverini, and A. Franchi. Experimental validation of a new adaptive control scheme for quadrotors MAVs. *IEEE/RSJ International Conference on Intelligent Robots and Systems*, pages 2439–2444, 2013. 11
- [33] E. Baird. A universal strategy for visually guided landing. *Proceedings of the National Academy of Sciences*, pages 1–15, 2013. 14
- [34] J. Blanco. A tutorial on se (3) transformation parameterizations and on-manifold optimization. Technical report, University of Malaga, Tech. Rep, 2010. 36
- [35] S. Bouabdallah. Design and Control of Quadrotors With Application To Autonomous Flying. Master’s thesis, ÉCOLE POLYTECHNIQUE FÉDÉRALE DE LAUSANNE, 2007. 10
- [36] S. Bouabdallah, a. Noth, and R. Siegwart. PID vs LQ control techniques applied to an indoor micro quadrotor. *IEEE/RSJ International Conference on Intelligent Robots and Systems (IROS)*, 3:2451–2456, 2004. 11
- [37] S. Bouabdallah and R. Siegwart. Full control of a quadrotor. *2007 IEEE/RSJ International Conference on Intelligent Robots and Systems*, (1):153–158, 2007. 11
- [38] H. Bouadi, M. Bouchoucha, and M. Tadjine. Sliding mode control based on backstepping approach for an UAV type-quadrotor. *World Academy of Science*, 1:1–6, 2007. 11
- [39] G. De Croon and M. Ieee. Controlling Spacecraft Landings With Constantly and Exponentially Decreasing. 51(2):1241–1252, 2015. 14
- [40] T. F. Delitalia. Modelling and control of 3DR IRIS Quadcopter. Unpublished, November 2014.

REFERENCES

- [41] J. Diebel. Representing attitude: Euler angles, unit quaternions, and rotation vectors. *Matrix*, 58:1–35, 2006. [37](#)
- [42] B. Erginer and E. Altug. Modeling and PD Control of a Quadrotor VTOL Vehicle. *2007 IEEE Intelligent Vehicles Symposium*, pages 894–899, 2007. [11](#)
- [43] M. Faessler, E. Mueggler, K. Schwabe, and D. Scaramuzza. A Monocular Pose Estimation System based on Infrared LEDs. *ICRA*, 2014.
- [44] J. Friis, E. Nielsen, R. F. Andersen, and A. Jochumsen. Autonomous Landing on a Moving Platform. Technical report, Aalborg University, Department of electronics systems, 2009. [15](#), [37](#)
- [45] D. Henderson. Euler Angles, Quaternions, and Transformation Matrices. *NASA JSC Report*, 1977.
- [46] B. Herisse, T. Hamel, R. Mahony, and F. X. Russotto. The landing problem of a VTOL unmanned aerial vehicle on a moving platform using optical flow. *IEEE/RSJ International Conference on Intelligent Robots and Systems, IROS*, 28(1):1600–1605, 2010. [15](#)
- [47] G. Hoffmann, H. Huang, and S. Waslander. Quadrotor helicopter flight dynamics and control: Theory and experiment. *American Institute of Aeronautics and Astronautics*, pages 1–20, 2007. [10](#)
- [48] H. Huang, G. M. Hoffmann, S. L. Waslander, and C. J. Tomlin. Aerodynamics and control of autonomous quadrotor helicopters in aggressive maneuvering. *Proceedings - IEEE International Conference on Robotics and Automation*, pages 3277–3282, 2009. [34](#)
- [49] D. Izzo and G. D. Croon. Landing with Time-to-Contact and Ventral Optic Flow Estimates. *Journal of Guidance, Control, and Dynamics*, 35:1362–1367, 2012. [14](#)
- [50] F. Kendoul, D. Lara, I. Fantoni, and R. Lozano. Real-Time Nonlinear Embedded Control for an Autonomous Quadrotor Helicopter. *Journal of Guidance, Control, and Dynamics*, 30(4):1049–1061, 2007. [42](#)
- [51] W. Khalil. *Modeling Identification and Control of Robots*. [36](#), [37](#)
- [52] T. Luukkonen. Modeling and control of Quadcopter. *Independent research project in applied mathematics*, 22:1134–45, 2011. [9](#)

REFERENCES

- [53] R. Mahony, V. Kumar, and P. Corke. Multirotor Aerial Vehicles: Modeling, Estimation, and Control of Quadrotor. *IEEE Robotics & Automation Magazine*, 19, 2012. [10](#), [11](#), [41](#)
- [54] D. Mellinger. Minimum snap trajectory generation and control for quadrotors. pages 2520–2525, 2012. [52](#)
- [55] Michael, Nathan. Quadrotor Modeling and Control. <http://www.cs.cmu.edu/afs/cs.cmu.edu/academic/class/16311/www/s15/syllabus/ppp/Lec08-Control3.pdf>, 2014. Accessed: 17-08-2015. [9](#)
- [56] J. F. Montgomery, A. H. Fagg, and G. a. Bekey. USC AFV-I: a behavior-based entry in the 1994 international aerial robotics competition. *IEEE expert*, 10:16–22, 1995. [13](#)
- [57] E. Mueggler, M. Faessler, F. Fontana, and D. Scaramuzza. Aerial-guided Navigation of a Ground Robot among Movable Obstacles. *SSRR Conference*, 2014.
- [58] M. Vendittelli. Elective in Robotics Quadrotor Modeling, Control Problems and approaches. [9](#), [40](#)
- [59] H. Voos. Nonlinear Landing Control for Quadrotor UAVs. Technical report, University of Applied Sciences Ravensburg-Weingarten, Mobile Robotics Lab, December 2008. [14](#)